VTRC
Virginia Transportation Research Council

We Bring Innovation to Transportation

Interstate 64 Pavement Recycling Instrumentation and Monitoring

https://vtrc.virginia.gov/media/vtrc/vtrc-pdf/vtrc-pdf/26-R19.pdf

CAROLINA BENAVIDES RUIZ, M.S., Graduate Research Assistant
Virginia Tech Transportation Institute

GERARDO W. FLINTSCH, Ph.D., P.E., Professor
Virginia Tech Department of Civil and Environmental Engineering

BRIAN K. DIEFENDERFER, Ph.D., P.E., Principal Research Scientist
Virginia Transportation Research Council

BILIN TONG, Ph.D., Postdoctoral Research Associate
Virginia Tech Transportation Institute

EUGENE AMARH, Ph.D., Senior Research Associate
Virginia Tech Transportation Institute

SAMER W. KATICHA, Ph.D., Research Scientist
Virginia Tech Transportation Institute

ILKER BOZ, Ph.D., P.E., Senior Research Scientist
Virginia Transportation Research Council

Final Report VTRC 26-R19

VIRGINIA TRANSPORTATION RESEARCH COUNCIL
530 Edgemont Road, Charlottesville, VA 22903-2454
vtrc.virginia.gov

Standard Title Page - Report on Federally Funded Project

1. Report No.: FHWA/VTRC 26-R19	2. Government Accession No.:	3. Recipient's Catalog No.:
4. Title and Subtitle: Interstate 64 Pavement Recycling Instrumentation and Monitoring		5. Report Date: October 2025
		6. Performing Organization Code:
7. Author(s): C.B. Ruiz, G.W. Flintsch, B.K. Diefenderfer, B. Tong, E. Amarh, S. Katicha, and I. Boz		8. Performing Organization Report No.: VTRC 26-R19
9. Performing Organization and Address: Virginia Transportation Research Council 530 Edgemont Road Charlottesville, VA 22903		10. Work Unit No. (TRAIS):
		11. Contract or Grant No.: 122323
12. Sponsoring Agencies' Name and Address: Virginia Department of Transportation 1221 E. Broad Street Richmond, VA 23219 Federal Highway Administration 400 North 8th Street, Room 750 Richmond, VA 23219-4825		13. Type of Report and Period Covered: Final Contract
		14. Sponsoring Agency Code:
15. Supplementary Notes: This is an SPR-B report.		

16. Abstract:

During the past two decades, the implementation of pavement recycling techniques, such as cold central plant recycling and full-depth reclamation, for pavement rehabilitation and construction in the United States has been driven by positive performance and the opportunity for significant cost and environmental savings. However, these recycling techniques are not commonly implemented because of the need for long-term performance information and a better understanding of the interactions between material properties, traffic configuration, and environmental conditions. This report presents the measured pavement responses (strains and stresses) of two recycled pavement sections on Interstate 64 in Virginia, incorporating cold central plant recycling and full-depth reclamation, which were subjected to real-world environmental and traffic-loading conditions. This work was completed to improve the understanding of the structural performance of pavements with recycled materials.

During this study, a suite of sensors—including strain gauges, pressure cells, thermocouples, and time domain reflectometry probes—was installed during the construction of two recycled pavement sections built on Interstate 64 near Williamsburg, Virginia. The first instrumented recycled pavement section was tested 13 times from 2019 to 2023, and the second recycled section was tested seven times from 2021 to 2023. Three to four trucks with known loading were driven over the instrumented sections during each field measurement event as part of the public traffic stream, and the responses from the instrumentation were recorded. In addition, the pavement structures were modeled using layered elastic software to compare the measured and calculated responses and refine the assumed mechanical properties of the materials used in the pavement structures. This study showed that the pavement sections had low strain, pressure, and deflection results and are expected to have a long structural life. The instrumentation was also found to be generally functional after 5 years and may be capable of providing additional performance information.

17. Key Words: Pavement recycling, CCPR, FDR, instrumentation, I-64	18. Distribution Statement: No restrictions. This document is available to the public through NTIS, Springfield, VA 22161.

19. Security Classif. (of this report): Unclassified	20. Security Classif. (of this page): Unclassified	21. No. of Pages: 62	22. Price:

FINAL REPORT

INTERSTATE 64 PAVEMENT RECYCLING INSTRUMENTATION AND MONITORING

Carolina Benavides Ruiz, M.S.
Graduate Research Assistant
Virginia Tech Transportation Institute

Gerardo W. Flintsch, Ph.D., P.E.
Director, Center for Sustainable Transportation Infrastructure
Virginia Tech Transportation Institute
Professor, Charles Via, Jr. Department of Civil and Environmental Engineering
Virginia Tech

Brian K. Diefenderfer, Ph.D., P.E.
Principal Research Scientist
Virginia Transportation Research Council

Bilin Tong, Ph.D.
Postdoctoral Research Associate
Virginia Tech Transportation Institute

Eugene Amarh, Ph.D.
Senior Research Associate
Virginia Tech Transportation Institute

Samer W. Katicha, Ph.D.
Research Scientist
Virginia Tech Transportation Institute

Ilker Boz, Ph.D., P.E.
Senior Research Scientist
Virginia Transportation Research Council

In cooperation with the U.S. Department of Transportation
Federal Highway Administration

Virginia Transportation Research Council
(A partnership of the Virginia Department of Transportation and the University of Virginia since 1948)

Charlottesville, Virginia

October 2025
VTRC 26-R19

DISCLAIMER

The contents of this report reflect the views of the author(s), who is responsible for the facts and the accuracy of the data presented herein. The contents do not necessarily reflect the official views or policies of the Virginia Department of Transportation, the Commonwealth Transportation Board, or the Federal Highway Administration. This report does not constitute a standard, specification, or regulation. Any inclusion of manufacturer names, trade names, or trademarks is for identification purposes only and is not to be considered an endorsement.

ABSTRACT

During the past two decades, the implementation of pavement recycling techniques, such as cold central plant recycling and full-depth reclamation, for pavement rehabilitation and construction in the United States has been driven by positive performance and the opportunity for significant cost and environmental savings. However, these recycling techniques are not commonly implemented because of the need for long-term performance information and a better understanding of the interactions between material properties, traffic configuration, and environmental conditions. This report presents the measured pavement responses (strains and stresses) of two recycled pavement sections on Interstate 64 in Virginia, incorporating cold central plant recycling and full-depth reclamation, which were subjected to real-world environmental and traffic-loading conditions. This work was completed to improve the understanding of the structural performance of pavements with recycled materials.

During this study, a suite of sensors—including strain gauges, pressure cells, thermocouples, and time domain reflectometry probes—was installed during the construction of two recycled pavement sections built on Interstate 64 near Williamsburg, Virginia. The first instrumented recycled pavement section was tested 13 times from 2019 to 2023, and the second recycled section was tested seven times from 2021 to 2023. Three to four trucks with known loading were driven over the instrumented sections during each field measurement event as part of the public traffic stream, and the responses from the instrumentation were recorded. In addition, the pavement structures were modeled using layered elastic software to compare the measured and calculated responses and refine the assumed mechanical properties of the materials used in the pavement structures. This study showed that the pavement sections had low strain, pressure, and deflection results and are expected to have a long structural life. The instrumentation was also found to be generally functional after 5 years and may be capable of providing additional performance information.

TABLE OF CONTENTS

FINAL REPORT

INTERSTATE 64 PAVEMENT RECYCLING INSTRUMENTATION AND MONITORING

Carolina Benavides Ruiz, M.S.
Graduate Research Assistant
Virginia Tech Transportation Institute

Gerardo W. Flintsch, Ph.D., P.E.
Director, Center for Sustainable and Resilient Infrastructure
Virginia Tech Transportation Institute
Professor, Charles Via, Jr. Department of Civil and Environmental Engineering
Virginia Tech

Brian K. Diefenderfer, Ph.D., P.E.
Principal Research Scientist
Virginia Transportation Research Council

Bilin Tong, Ph.D.
Postdoctoral Research Associate
Virginia Tech Transportation Institute

Eugene Amarh, Ph.D.
Senior Research Associate
Virginia Tech Transportation Institute

Samer W. Katicha, Ph.D.
Research Scientist
Virginia Tech Transportation Institute

Ilker Boz, Ph.D., P.E.
Senior Research Scientist
Virginia Transportation Research Council

INTRODUCTION

During the past two decades, the implementation of recycled techniques for pavement rehabilitation and construction in the United States has been driven by positive performance, environmental awareness, and the opportunity for significant cost savings (Diefenderfer et al., 2016a; FHWA, 2022; Jain and Singh, 2021; Williams et al., 2019). The emerging pavement recycling techniques, such as cold central plant recycling (CCPR) and full-depth reclamation (FDR), efficiently use resources, reduce residual waste, and lower greenhouse gas emissions compared with hot-mix asphalt, leading to more sustainable pavements (Bressi et al., 2019; Chavez et al., 2019; Liu et al., 2014; Moreno-Navarro et al., 2015). However, these recycled

methods are not commonly implemented in high-volume routes because of the need for more detailed performance information and understanding of the interactions between material properties and environmental conditions (Timm et al., 2018; Zimmerman, 2017).

The Virginia Department of Transportation (VDOT) has been studying the performance of pavement recycling techniques since 2008 to address the lack of information on recycling techniques for pavements. One of the first studies conducted by VDOT involved reconstructing a section of Interstate 81 (I-81) using cold in-place recycling, CCPR, and FDR. The study examined pavement performance in terms of structural capacity measured with a falling weight deflectometer (FWD) (Diefenderfer et al., 2012).

In 2012, VDOT further evaluated the functional and structural performance of three test sections at the National Center for Asphalt Technology (NCAT) Test Track. These sections were constructed with CCPR and FDR processes to investigate the effect of asphalt thickness and the presence of a stabilized foundation on the CCPR layer under accelerated pavement testing. The results showed excellent performance across multiple test cycles. Initially, all sections (N3, N4, and S12) successfully handled 10 million equivalent single-axle loads (ESALs) from 2012 to 2014 and then 20 million ESALs from 2015 to 2017, without exhibiting any cracking or distress (Timm et al., 2015; Timm et al., 2018). Consequently, Section N3 was discontinued, and the structurally extreme sections (thickest and thinnest overall cross sections, S12 and N4, respectively) continued testing. Sections S12 and N4 were subjected to further loading, reaching 30 million ESALs by 2021, at which point S12 was discontinued without any observable surface distress (Bowers et al., 2022; West et al., 2024). Finally, N4, the thinnest section, sustained loading up to 40 million ESALs, with the first cracks appearing at 29.7 million ESALs (West et al., 2024). In addition, the performance of these three sections was documented by analyzing the results of deflection testing using FWD, stress and strain measurements from instrumentation, and surface deterioration (Diefenderfer et al., 2019). In addition, the structural layer coefficients of CCPR were determined using empirical pavement design concepts and FWD test results. The structural layer coefficients ranged from 0.30 to 0.35 based on empirical design concepts and 0.36 to 0.39 based on FWD test results (Diefenderfer et al., 2016b; Díaz Sánchez, 2019).

In 2015, two pavement test sections with CCPR as base layers were constructed at the Virginia accelerated pavement testing facility to investigate the optimal overlay thickness (Flintsch et al., 2020). The findings suggested that using thinner surface layers in CCPR pavements resulted in concentrated wheel loads over smaller areas in the layers below, potentially increasing vertical pressure, shear stress, and rutting. Furthermore, Amarh (2017) showed that the stiffness of the recycled mixtures increased over time, based on FWD tests.

VDOT continued its research efforts in 2018 with the instrumentation of two segments as part of the Interstate 64 (I-64) widening and reconstruction projects near Williamsburg, Virginia. A 7.06-mile section (Segment II) and an 8.2-mile section (Segment III) spanning Newport News, York, and James City Counties were widened and reconstructed. The work included two recycling techniques, CCPR and FDR. A new travel lane and inside shoulder were constructed on the center-median side of the existing pavement, and the existing two lanes and outside shoulder were reconstructed. The project team installed instrumentation during the construction phase on westbound I-64 between Exits 242B and 242A for Segment II and on eastbound I-64

between Exits 234 and 238 for Segment III. According to VDOT's average annual daily traffic reports from 2018 to 2021, both segments carried approximately 40,000 vehicles per day, with trucks comprising 5 to 8% of the total traffic. The instrumentation was used to monitor and analyze the response of these two recycled pavement sections under environmental conditions and traffic loading (Benavides-Ruiz, 2021; Diefenderfer et al., 2023; Flintsch et al., 2020).

PURPOSE AND SCOPE

The purpose of this study was to understand the behavior of two pavement sections (Segments II and III) better that were instrumented and constructed using CCPR and FDR on I-64 in Virginia between 2017 and 2021. The pavement sections were tested between 2019 and 2023 for Segment II and between 2021 and 2023 for Segment III during a series of measurement events during which loaded trucks passed over the instrumented sections. These measurement events were conducted across different seasons to capture pavement responses across different environmental conditions.

METHODS

To achieve the purpose of this study, the following tasks were performed:

1. Conducting a literature review on the recent performance of recycled pavement projects and perpetual pavements.
2. Installing instruments to measure strain, pressure, temperature, and moisture during the construction of two test sections on I-64.
3. Summarizing the response of the pavement test sections subjected to loaded trucks under actual environmental and traffic speed conditions.
4. Comparing the measured pavement responses with those calculated through modeling, using an open-source layered elastic analysis software (OpenPave, 2025).

Pavement Sections

The two experimental instrumented sections were within Segments II and III of the I-64 widening and reconstruction project (Figure 1). The pavement structure for both segments consisted of the following four layers placed on top of the native subgrade: asphalt concrete (AC), CCPR, open-graded drainage layer (OGDL), and FDR. The AC layer was composed of two stone matrix asphalt layers with a nominal maximum aggregate size of 12.5 mm and 19 mm, and a performance-grade 76-22 asphalt binder (Bruns, 2021; VDOT, 2019). The CCPR material was a blend of 85% reclaimed asphalt pavement and 15% No. 10 aggregate, and it was stabilized with 2.5% foamed performance-grade 64-22 asphalt binder and 1% Type II Portland cement (Bowers et al., 2019; FHWA, 2020). OGDL had a nominal maximum aggregate size of 19 mm and used performance-grade 64E-22 asphalt binder (Bruns, 2021). The FDR layer was comprised of imported crushed concrete for the new lanes and the existing aggregate base and top portion of the existing subgrade for the existing lanes. Both sections were stabilized with 5% Portland cement (FHWA, 2020).

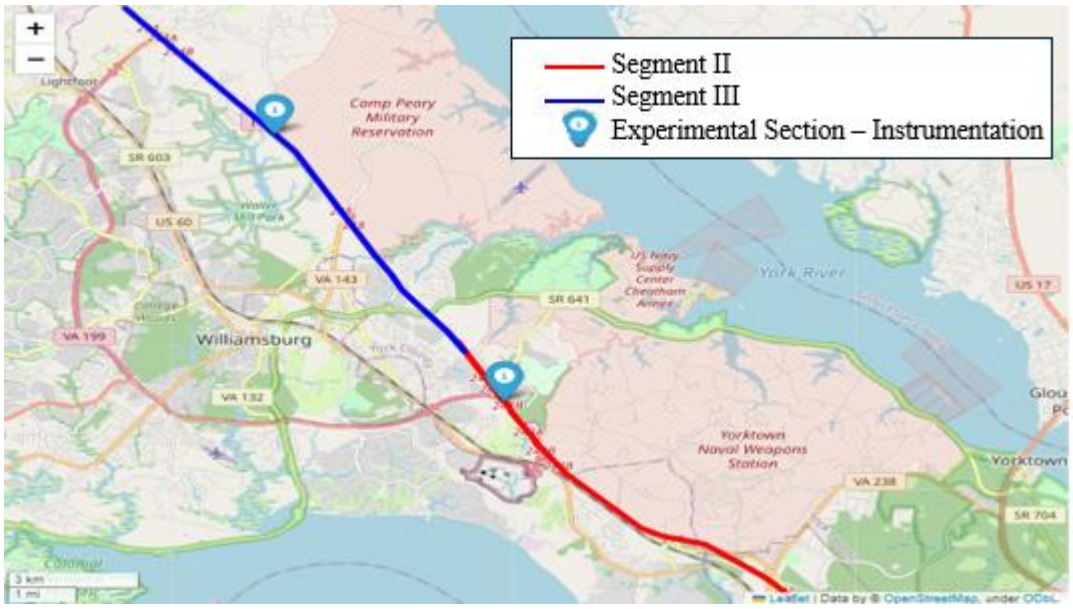

Figure 1. Interstate 64 Widening Project in Newport News, York, and James City Counties

The pavement design for each segment was based on agency guidelines and lessons learned from previous pavement recycling projects, including the portion of I-81 constructed in 2011 (Diefenderfer et al., 2012) and the VDOT-sponsored sections at the NCAT Test Track constructed in 2012 (Timm et al., 2015; Timm et al., 2018). Figure 2 shows the cross section for I-81, the NCAT test sections, and the I-64 Sections II and III. The I-64 projects feature a design modification in which an asphalt-stabilized OGDL was added to improve drainage within the pavement structure.

Material Characterization

To model the response of the pavement sections, the mechanical properties of the various layers were obtained from two different sources. For the CCPR and FDR layers, properties of similar materials used in Virginia pavement sections constructed at the NCAT Test Track were used (Bowers et al., 2019). For the AC layer and OGDL, the AASHTOWare pavement materials files, published by VDOT, were used to construct master curves at a reference temperature of 70°F (VDOT, 2017). The master curves were constructed using the sigmoidal function presented in Equation 1. Table 1 shows the fitted parameters of the master curve along with binder viscosity parameters.

$$\log E = \delta + \frac{\alpha}{1+e^{\beta+\gamma\, log(tr)}} \qquad \text{Equation 1}$$

Where:
E = dynamic modulus (psi).
tr = loading time to reference temperature (seconds).
α, β, γ, δ = fitting coefficients.

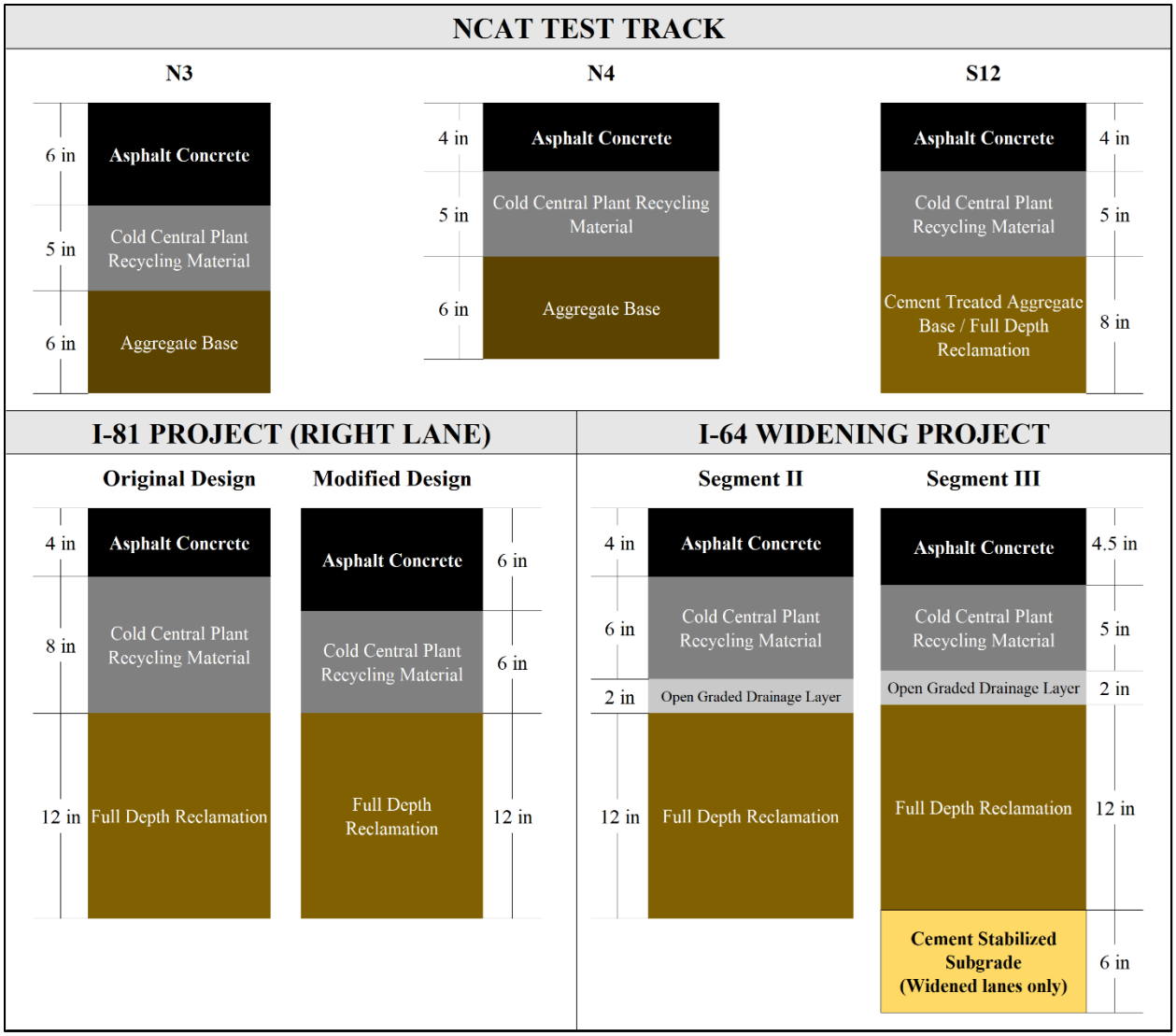

Figure 2. Cross Sections of Interstate 81, NCAT Test Sections, and Interstate 64 Projects Showing Design Thicknesses. NCAT = National Center for Asphalt Technology.

Table 1. Master Curve Parameters

Layer	Master Curve-Fitting Coefficients						Binder Characteristics		
	α	β	γ	δ	C	R^2	A	VTS	Reference Temperature (°F)
SMA	2.9952	– 0.88682	0.35357	3.74119	1.20204	0.99	9.925	– 3.285	70
CCPR	2.3438	– 1.69682	0.31611	3.63271	1.01884	0.99	10.980	– 3.680	70
OGDL	2.0921	– 0.28307	0.40078	4.16864	1.16486	0.99	10.980	– 3.68	70

CCPR = cold central plant recycling; OGDL = open-graded drainage layer; SMA = stone matrix asphalt; VTS = viscosity-temperature susceptibility.

For the FDR layers, VDOT currently assumes their behavior can be modeled either as non-stabilized base layers for flexible pavements with an estimated resilient modulus of 80,000 psi or as a chemically stabilized layer with an elastic and resilient modulus of 750,000 psi (VDOT, 2017).

Pavement Instrumentation

During construction of Segments II and III, pressure cells, strain gauges, thermocouples, and moisture sensors were installed. The sensors were placed in the right wheel path of the right lane of both sections. Figures showing the construction and installation processes are provided in Appendix A. Researchers used a National Instruments Corporation data acquisition system (DAS) during each field measurement event to collect the signals obtained from the instrumentation. Table 2 presents a summary of the instrumentation placed in each segment, and Figure 3 shows the plan and profile views. Appendix B provides more information regarding the instrumentation.

Table 2. Instrumentation Summary

Sensor	Manufacturer	Model	Quantity Used in Segment II	Quantity Used in Segment III
Strain Gauge	Tokyo Sokki Kenkyujo Co., Ltd.	KM-100HAS	9	9
Pressure Cell	Geokon, Inc.	3500	6	3
Thermocouple	Pyromationnon, Inc.	T (E230)	6	6
Moisture Sensor	Decagon Devices, Inc.	Model GS1	3	2

In both segments, nine strain gauges were placed at the bottom of the CCPR layer in three groups (three replicate gauges each at left, center, and right side of the right wheel path) to measure the longitudinal strain and account for the wheel wander of the trucks running at traffic speed. In Segment II, pressure cells were installed at the bottom of the CCPR layer and at the top of the subgrade to analyze and compare the distribution of vertical stresses within the pavement structure. In Segment III, however, pressure cells were installed on top of the subgrade only. This decision was based on the insights gained from Segment II and considerations regarding sensor durability because one of the pressure cells installed at the bottom of the CCPR in Segment II was damaged during construction.

Thermocouples and moisture sensors were installed at different depths to monitor the pavement temperature gradient and the moisture content. In Segment II, the thermocouples were positioned at depths of 2, 5, and 7 inches from the pavement surface to measure the pavement temperature within the asphalt-bound layers, which are sensitive to temperature variations. Moisture sensors were placed at depths of 10, 24, and 48 inches from the pavement surface to monitor the moisture levels at the bottom of the CCPR layer, the bottom of the FDR, and 24 inches into the subgrade. These three depths help identify excess moisture in the subgrade, which can compromise its load-bearing capacity. In addition, they provide information for evaluating the effectiveness of the drainage system within the pavement structure.

In Segment III, the thermocouples were placed at a depth of 5.75 inches from the pavement surface to measure the mid-depth pavement temperature within the CCPR layer. Moisture sensors were installed at 23.5 and 47.5 inches to obtain the moisture content at the top of the FDR and 24 inches into the subgrade.

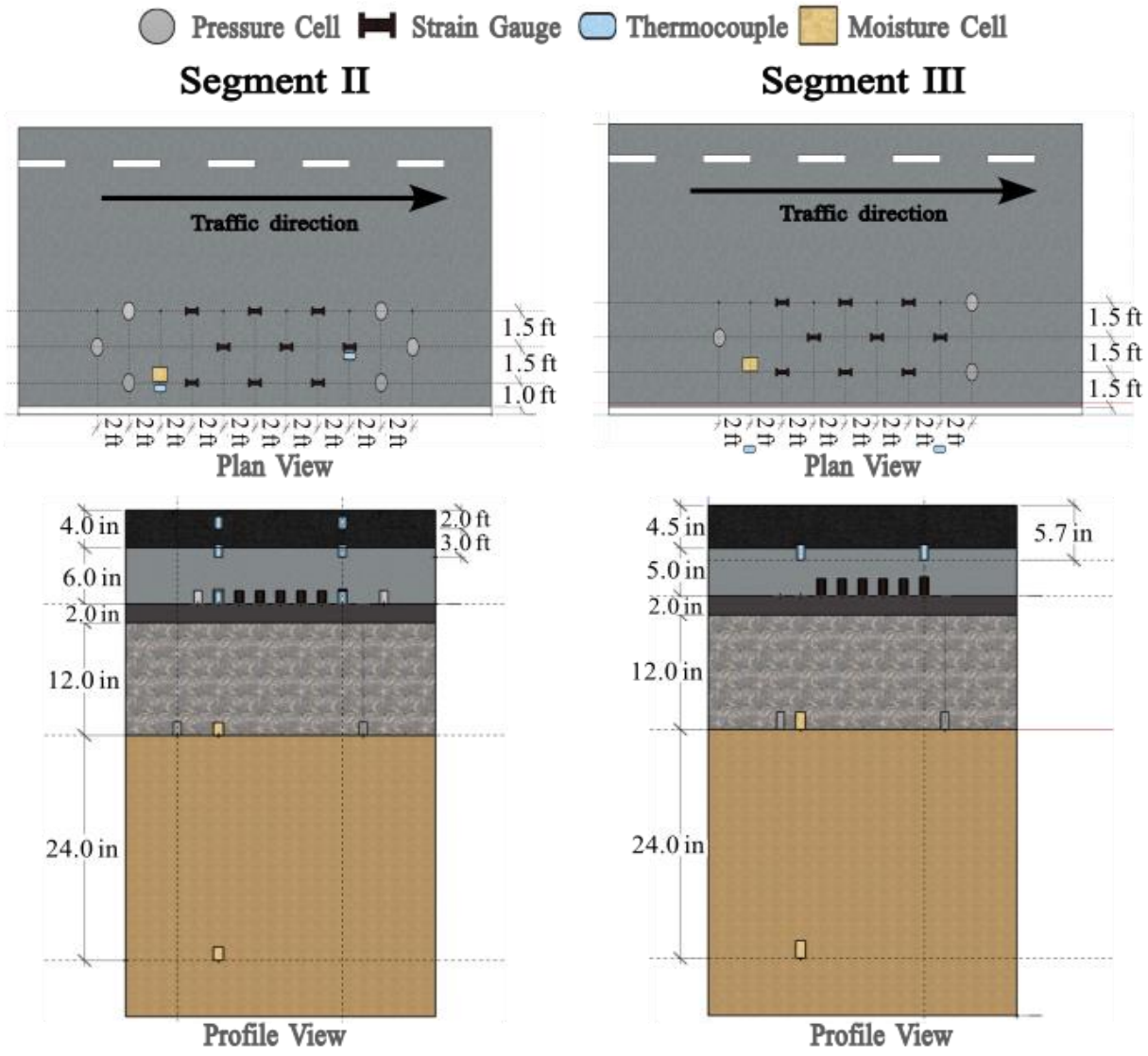

Figure 3. Instrumentation Layout Segments II and III

Load Testing

The load testing involved collecting data from multiple field measurement events, in which three to four loaded trucks passed over the instrumented pavement sections 12 to 20 times per event on the two segments of the I-64 widening projects. These measurements took place on different dates to capture seasonal variations of the pavement response throughout the year. Segment II, which was constructed first and completed in April 2019, underwent testing approximately every month during its first year, then every 3 to 4 months thereafter. Segment III, whose construction began after Segment II, was completed in November 2021 and underwent testing every 3 to 4 months. Before each field measurement event, the research team measured the static weight of each truck's wheels using portable scales, connected the embedded pavement sensors to DAS, and used a video camera to identify which vehicle passed over the instrumented sections.

The trucks used in each field measurement event featured either two axles (steering axle and single axle with dual tires) or three axles (steering axle and a tandem axle with dual tires) (Figure 4). For each measurement event, each truck was loaded with aggregate or other available material until the truck weighed approximately 31,000 pounds for the two-axle truck and approximately 43,000 pounds for the three-axle truck.

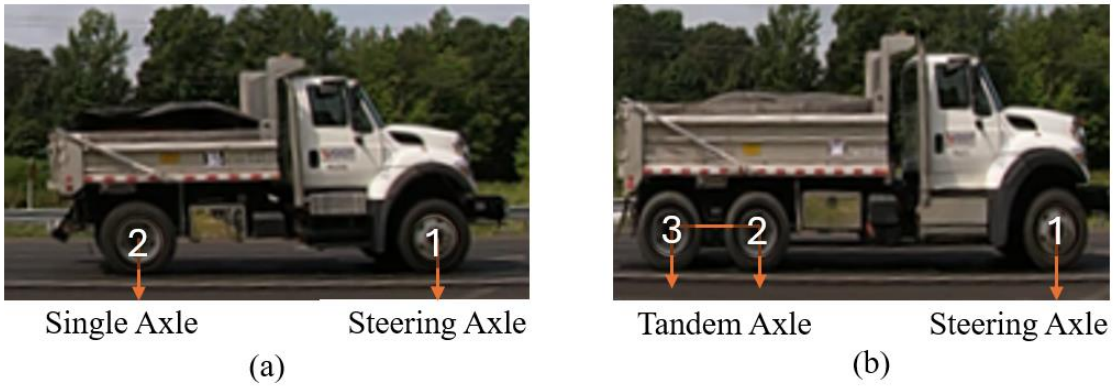

Figure 4. Trucks Used with (a) Two-Axle or (b) Three-Axle Configuration

Error! Not a valid bookmark self-reference. summarizes the key characteristics of the trucks used during the field measurements, including the average load per axle and the overall average weight for each truck type. In addition, Table 3 includes the average load on the right side of the axle because this side was the load that passed over the instrumented section and was used for load normalization, which is explained in a subsequent section. The static weight of each half axle was measured separately before each field measurement (Figure 5), using portable scales and recorded (Figure 6). All recorded truck weights are summarized in Appendix C.

Table 3. Loaded Truck Summary

Truck Type	Axle	Average Load, Right Side (lbs.)	Average Total-Axle Load (lbs.)	Average Total Truck Load (lbs.)
Two Axle	1st	5,392	11,148	31,258
	2nd	9,916	20,110	
Three Axle	1st	6,880	13,983	43,583
	2nd	7,353	14,840	
	3rd	7,067	14,760	

Figure 5. (a) Truck Loading Loaded with Sand and (b) Axles Weight Measurement

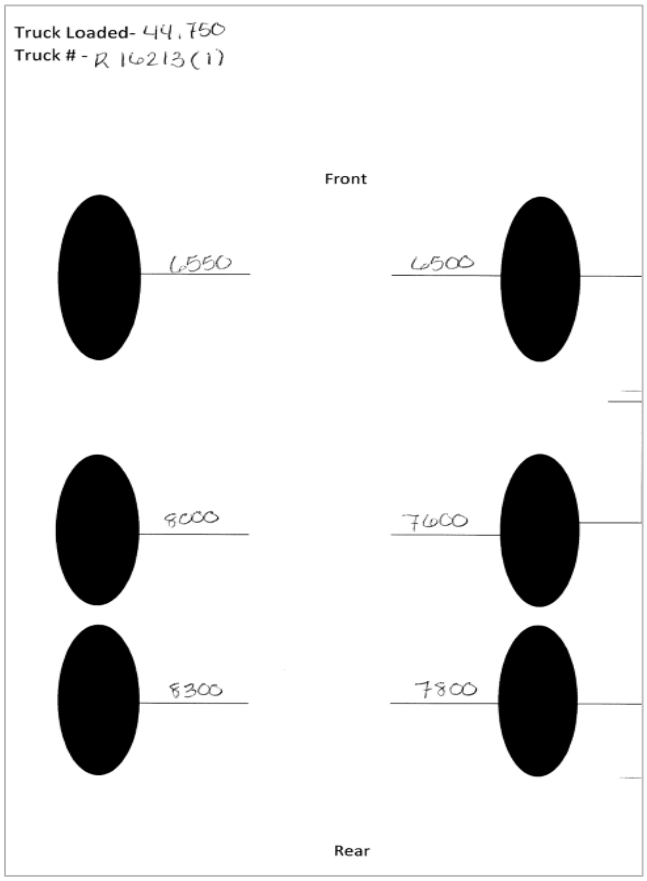

Figure 6. Example of Truck Weight Data Sheet

Data Collection and Analysis

Moisture and Temperature Data

The moisture content and pavement temperature were recorded for each measurement event. A total of 263 moisture content values were recorded for Segment II, and 208 moisture content values were recorded for Segment III. The difference in the number of responses recorded per segment is due to changes in the data collection process. In Segment II, during the field measurements performed in 2019, moisture content was recorded only during the first and last run of each data collection session. However, starting in 2021, the procedure was changed to record the moisture content every time the trucks passed over the section. This change was made based on increased DAS channels available to connect to the sensors. A representative moisture content for each field experiment was calculated by calibrating the sensor readings according to the manufacturer's specifications and then by calculating the average of these calibrated responses.

The minimum, maximum, and average air temperature values were collected from the U.S. weather station—the Walnut Hills Station—nearest to the project segments during the day of each field measurement event. Pavement temperatures were measured using the

thermocouples embedded within the pavement layers. A representative pavement temperature at each depth for every field measurement event was calculated as the average recorded value from each truck pass.

Pavement Response Data

The instrumented section in Segment II was tested 13 times between 2019 and 2023, and Segment III was tested seven times from 2021 to 2023. Three or four loaded trucks drove over the instrumented sections between 12 and 20 times during each measurement event. Most measurements were conducted from 9:30 a.m. to 1:30 p.m. Table 4 provides a summary of the field measurement events. The number and configuration of trucks were determined based on availability when each measurement event occurred.

Table 4. Field Measurement Events

Year	Month	Number of Two-Axle Trucks	Number of Three-Axle Trucks	Number of Passes per Truck	
				Segment II	Segment III
2019	June	1	2	12	-
	August	2	1	12	-
	September	3	0	12	-
	November	2	1	20	-
	December	3	0	16	-
2021	April	4	0	20	-
	November	0	3	18	14
2022	April	2	1	20	15
	August	1	2	18	17
	November	2	1	16	13
2023	March	2	1	16	16
	August	1	2	15	15
	November	2	1	15	15

Before each field measurement event, the sensors embedded in the pavement were connected to the DAS (Figure 7), and a video camera was set up to record the traffic passing over the section. The recording was used to match the type of truck passing over the instrumented section with the measured response of the embedded sensor, ensuring accurate analysis and preventing misleading results in cases when other trucks or vehicles may have passed between the known load trucks. Figure 8 shows a portion of one video.

Figure 7. Sensors Connected to the Data Acquisition System

Figure 8. Example of a Truck Passing over the Instrumented Section

A MATLAB script was developed to process the strains and stresses recorded by the DAS. The script extracted the peak stress values from each pressure cell for every axle pass of each truck and identified the maximum and minimum strain values recorded by each strain gauge. Figure 9 shows an example of the strain response for a two-axle truck, as measured by strain gauges EKZ151728 and EKZ151701, which are at the left of the wheel path (Segment II). The total strain, representing the elastic strain response of pavement, is calculated as the

difference between the maximum compressive strain and the maximum tensile strain, with these values highlighted by circles on each strain gauge trace in Figure 9.

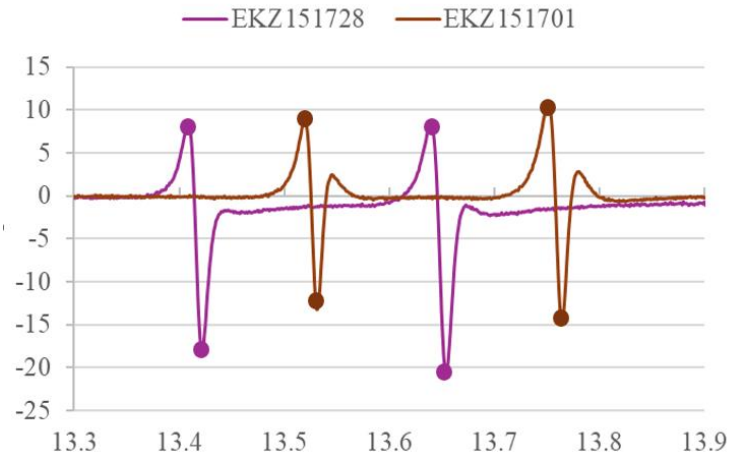

Figure 9. Strain Responses Collected in August 2023—Segment III

To compare the pavement responses collected at different temperatures and load conditions, the research team normalized the strains and stresses to a reference load using Equations 2 and 3, respectively. The reference half-axle loads were 5,300 pounds for the steering axle of both truck configurations, 9,800 pounds for the rear axle of the single-dual tire axle truck configuration, and 7,600 pounds for each of the two rear axles (lead and trailing) of the tandem axle truck configuration. These values represent the average load per half axle on the right side recorded for the different trucks operating over the sections during the field measurement events.

$$\varepsilon_N = \varepsilon \times \frac{P_N}{P} \qquad \text{Equation 2}$$

Where:
ε_N = normalized microstrain measured at reference load.
ε = microstrain measured by load P.
P_N = reference load (lb).
P = applied load on the right side of the axle (lb).

$$\sigma_{zN} = \sigma \times \frac{P_N}{P} \qquad \text{Equation 3}$$

Where:
σz_N = normalized compressive vertical stress measured at reference load (psi).
σ = compressive stress measured by load P (psi).
P_N = reference load (lb).
P = applied load on the right side of the axle (lb).

The data were temperature normalized using the methodology outlined by Timm (2020). This process involved the following steps:

- Data Grouping: Grouping the strain (total and tensile) or stress data based on the axle type.
- Curve Fitting: Fitting exponential trendlines to the grouped data, obtaining a curve that represents how strain and stress change with temperature.
- Response Normalizing: Using the equation from an exponential trendline to determine the response at 68°F.
- Representative Response Selection: Selecting the 95th percentile value from each field measurement event as the representative response under the corresponding axle type. This selection ensures proximity to the highest response and removes processing mistakes caused by processing errors, voltage spikes, or wheel wander.

Additional details of this process can be found in the Results section of this report.

Data Validation

The research team modeled the pavement sections using the layered elastic software OpenPave to validate the measured strain (total and tensile) responses and the material properties that characterized the pavement structures. This analysis focused on the responses from two-axle trucks, the predominant vehicle type used in most of the field measurement events.

The modulus for each asphalt-bound layer (stone matrix asphalt, CCPR, and OGDL) was calculated through a master curve analysis at a reference temperature of 68°F and a loading time determined using Equation 4 with a vehicle speed of 55 mph.

$$\log(t) = 0.5d - 0.2 - 0.94\log(v) \qquad \text{Equation 4}$$

Where:
t = loading time (sec).
d = pavement depth (m).
v = vehicle speed (km/h).

For the subgrade, an A-6 soil type was assumed (Hossain, 2010). For the FDR layer, two different scenarios for the resilient modulus were considered based on the *AASHTOWare Pavement ME User Manual* (VDOT, 2017). One scenario assumes a resilient modulus of 80,000 psi, which is close to the estimated modulus for FDR as a non-stabilized base layer. In contrast, the other assumes a resilient modulus of 750,000 psi, representing the estimated modulus for cement-treated FDR as a chemically stabilized layer.

The strain responses were normalized to the pavement temperature of 68°F. The steering axle received a load of 5,300 pounds, and the single-dual tire axle received a load of 4,900 pounds (per tire). In addition, a tire pressure of 750 kPa was assumed.

Regarding the point analysis, the longitudinal strain was measured at the bottom of the CCPR layer under the wheel for the steering axle. In contrast, strain was estimated both under the wheel and between the two wheels for the single-dual tire axle. These results were compared with the strain values recorded by gauges.

RESULTS AND DISCUSSION

Moisture and Temperature Data

Figure 10 presents the average measurements of the three moisture gauges installed at Segment II and the two gauges installed at Segment III. As Figure 10 shows, the moisture content within Segment II presented a relatively stable trend at each specific depth during the initial 3 years: 20% at 10 inches, 32% at 24 inches, and 38% at 48 inches. As expected, these measurements indicated that moisture content increases with depth, with the highest levels recorded 2 feet within the subgrade and the lowest values at the bottom of the CCPR layer. However, starting in November 2022, an increase in the moisture measured at 10 inches was observed. This increase could be attributed to a reduction in the OGDL's permeability due to clogging or sensor damage (Hajek et al., 1992). In Segment III, a greater variability in measured moisture was observed, with differences between consecutive measurements ranging from 1 to 6%. The highest variations were observed during the spring, with differences of 3.7% in April 2022 and 5.5% in March 2023. The average moisture content measured was 24% at a depth of 23.5 inches and 26% at a depth of 47.5 inches.

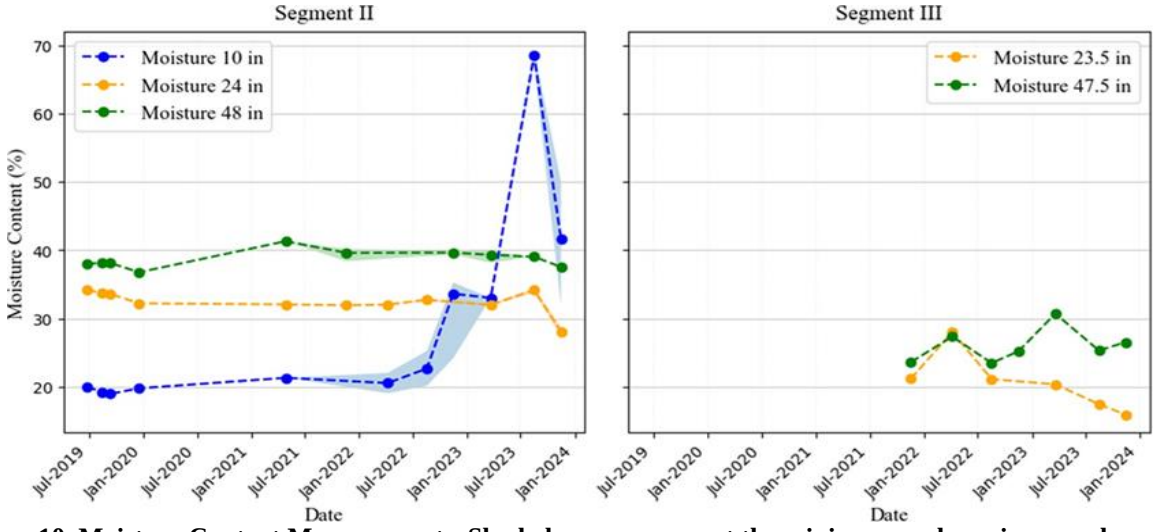

Figure 10. Moisture Content Measurements. Shaded areas represent the minimum and maximum values recorded in each field measurement.

The noise level was estimated using the root mean square of the error to evaluate the sensors' performance in Segment II. Table 5 shows a noticeable increase in noise levels over time for the sensor located at 10 inches, suggesting potential sensor degradation. Noise levels were stable between 1.2×10^{-4} and 1.9×10^{-4} from June to December 2019. However, a progressive increase is present starting in April 2021, with the noise level peaking at 7.4×10^{-3} in March 2023.

Table 5. Noise Level Moisture Sensors—Segment II

Date	Moisture 10-Inch Mean Noise	Moisture 24-Inch Mean Noise	Moisture 48-Inch Mean Noise
June 2019	1.2E-04	1.3E-04	9.2E-05
August 2019	1.9E-04	2.6E-04	1.9E-04
September 2019	1.9E-04	1.4E-04	1.5E-04

Date	Moisture 10-Inch Mean Noise	Moisture 24-Inch Mean Noise	Moisture 48-Inch Mean Noise
December 2019	1.5E-04	1.2E-04	1.2E-04
April 2021	3.3E-04	1.5E-04	9.8E-04
November 2021	-	5.6E-04	1.6E-03
April 2022	6.5E-04	2.7E-04	-
August 2022	1.3E-03	2.3E-04	-
November 2022	3.2E-03	-	7.1E-04
March 2023	7.4E-03	2.7E-04	7.2E-04
August 2023	4.0E-04	3.8E-04	3.6E-04
November 2023	6.6E-03	8.8E-04	1.6E-04

Figure 11 shows the average air temperature readings from the Walnut Hills Weather Station. The dates for the testing events were selected to evaluate the pavement responses at different temperatures throughout the year, capturing seasonal variations in summer, spring, fall, and winter. Figure 11 also shows the average air temperature in November 2021 exceeded the high average monthly temperature.

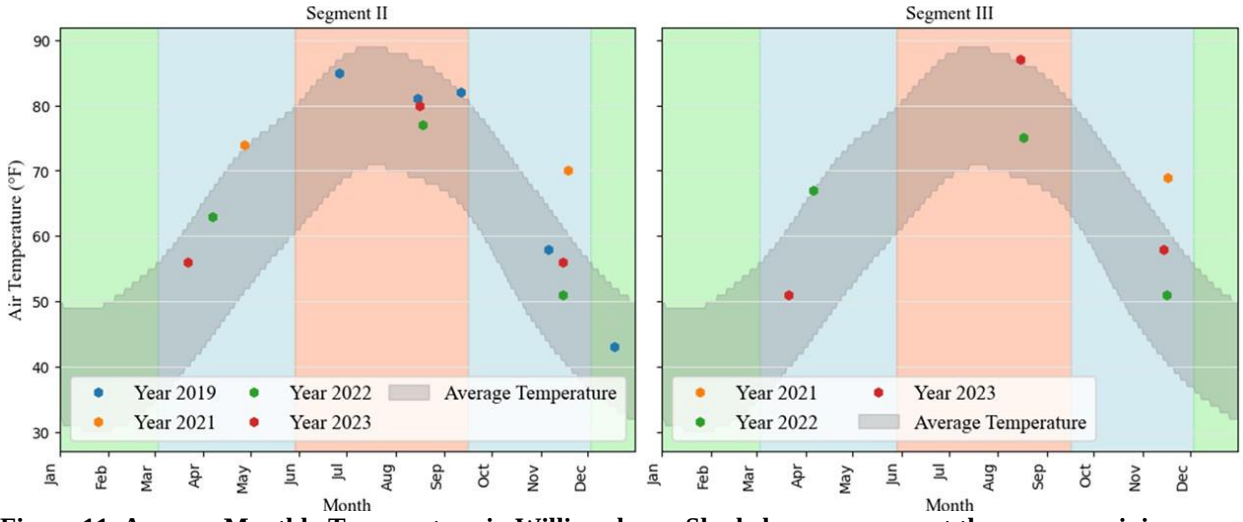

Figure 11. Average Monthly Temperature in Williamsburg. Shaded areas represent the average minimum and maximum air temperature values recorded by Walnut Hills Weather Station.

Regarding the temperature measurements, Figure 12 shows the average temperature of each test date for the six thermocouples installed in both segments. The temperature varied monthly, with the highest values observed in June and the lowest in December. A relationship between air temperature and pavement temperature is presented in Appendix D. As expected, the thermocouples in Segment II in the AC layer recorded higher temperatures compared with those in the CCPR layer. In addition, the temperature readings at the same depth showed consistent trends over time. For Segment III, all thermocouples were installed at the same depth, which explains why all the sensors gave close temperature readings.

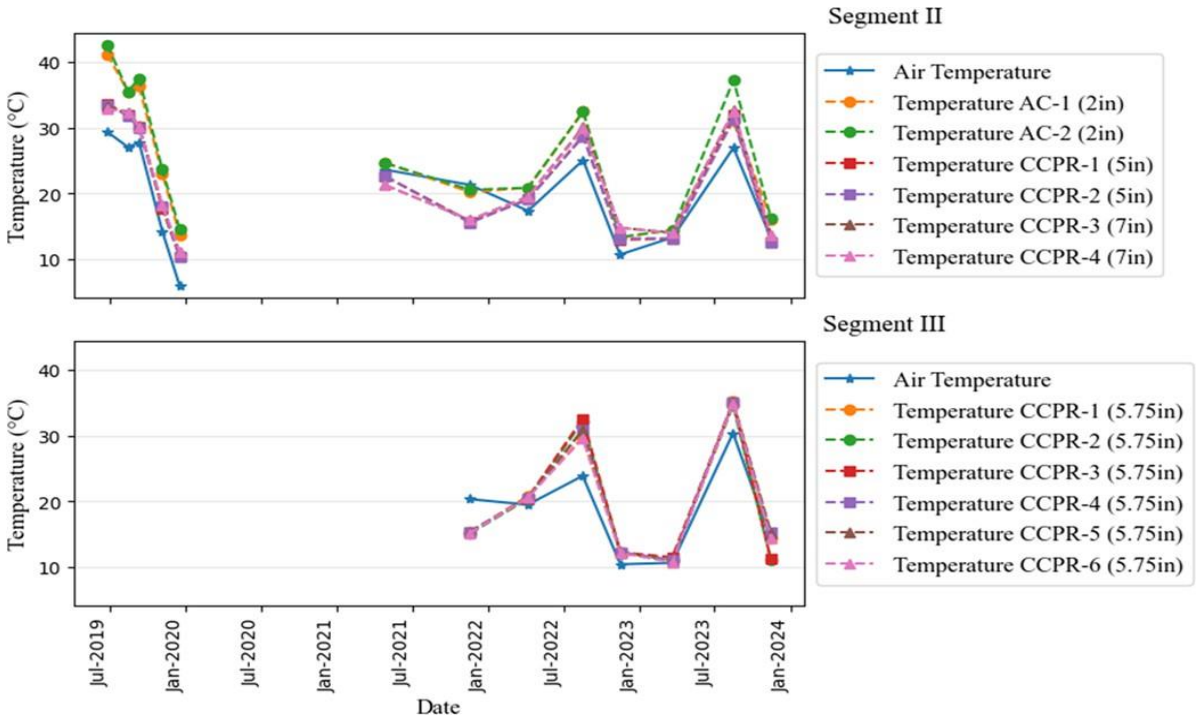

Figure 12. Temperature Measurements for Segments II and III. In the legend, each label specifies the pavement layer where the sensor was installed. The number following the layer name distinguishes between multiple sensors positioned at the same depth, and the value in parentheses indicates the depth of the sensor in inches. AC = asphalt concrete; CCPR = cold central plant recycling.

Pavement Responses

Total Strain

Strain responses recorded during the tests were analyzed to evaluate how traffic loading and environmental conditions (mainly temperature) affect the response of the pavement system. During each measurement event, the strain responses were recorded at the bottom of the CCPR layer for each pass of the testing trucks. The strain responses were reported as total strain, that is, the difference between the maximum compressive and maximum tensile strain from each pass. Considering that the trucks featured two or three axles and, because each type of axle generated different strain levels in the pavement, the following analysis separates the responses by vehicle type. In addition, responses from each field measurement event showed significant variability because of the challenges of truck wander, temperature variations, and voltage spikes from sensors (Figure 13).

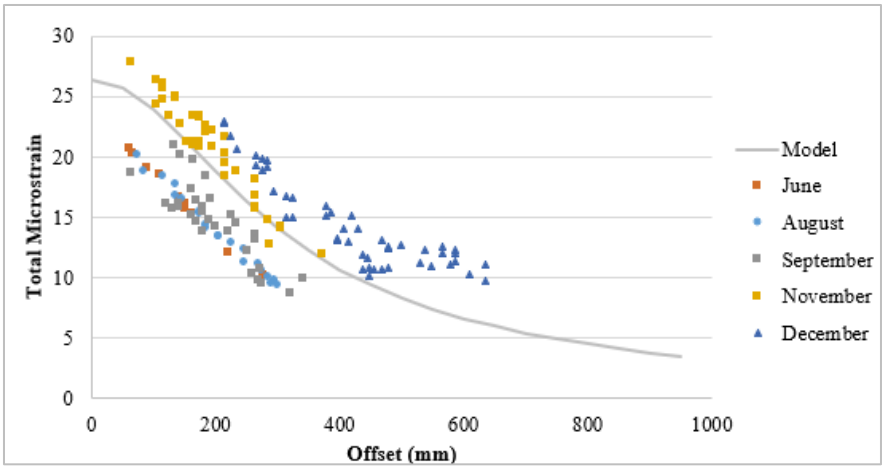

(a)

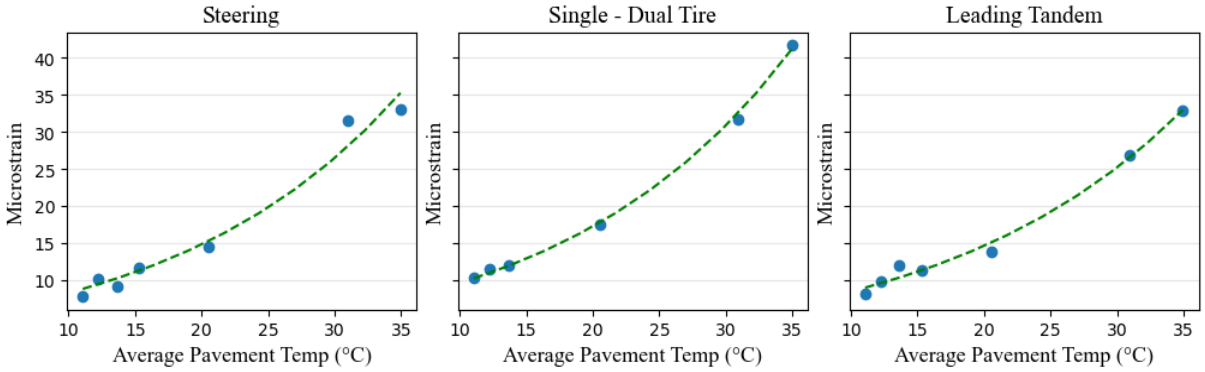

(b)

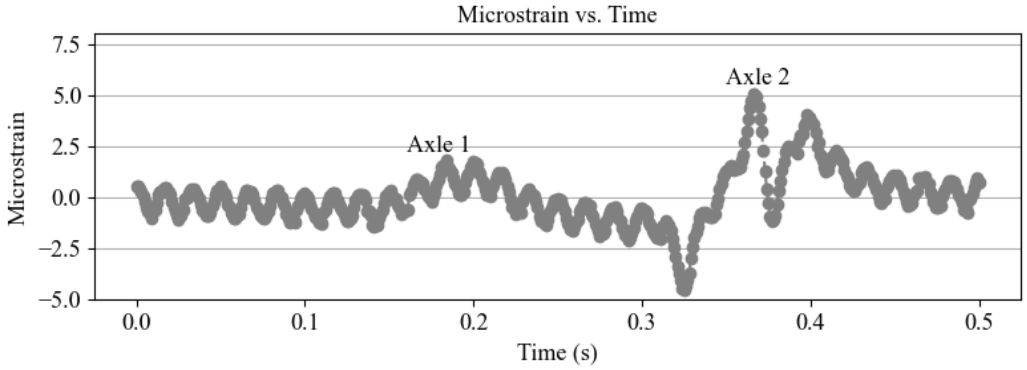

(c)

Figure 13. Examples of Wander, Temperature, and Voltage Spikes on Total Strain at the Bottom of the Cold Central Plant Recycling Layer: (a) Wheel Wander Effect on Total Strain Measurements—Segment II, Year 2019; (b) Total Strain Measurements and Average Pavement Temperature Relationship—Segment III; (c) Voltage Spikes November 2023, Test 1 Sensor EKZ151732 (Left-Side Wheel Path)

For each testing date and axle type, the peak total strain responses were identified for each pass of each axle from the vehicles used. Because multiple loading passes were conducted during each field measurement event, several peak strain responses were available for each axle. To select a representative response for each testing date, the 95th percentile was calculated,

meaning the calculated value is greater than 95% of all recorded responses for each axle type on that date.

A temperature correction based on regression was performed to normalize the strain responses with respect to temperature (Appendix E). The correlation equation from the regression analysis and the coefficient of correlation obtained are presented in Equation 5 and Table 6, respectively.

$$\varepsilon_T = k_1 \times e^{T \times k_2} \quad \text{Equation 5}$$

Where:
ε_T = microstrain measured at temperature, T.
k_1 and k_2 = regression coefficients.
e = exponential constant (2.718282).
T = mid-depth pavement temperature.

Table 6. Summary of Total μstrain and Average Pavement Temperature Relation—Bottom Cold Central Plant Recycling Layer

Axle Type		Regression				
		Observations	k_1	k_2	R-squared	p-value k_2
Segment II	Steering	11	10.71	0.035	0.89	8.4×10^{-6}
	Single-Dual Tire	8	24.78	0.017	0.70	5.6×10^{-3}
	Tandem (Leading axle)	8	15.64	0.029	0.74	5.7×10^{-3}
Segment III	Steering	7	4.67	0.058	0.97	3.7×10^{-5}
	Single-Dual Tire	6	5.41	0.058	0.99	7.1×10^{-7}
	Tandem (Leading axle)	7	4.96	0.054	0.99	2.7×10^{-5}

The exponential regression summary, as shown in Table 6, indicates a strong positive relationship between temperature and pavement strain response, evidenced by high R^2 values, and a statistically significant influence of temperature, based on p-values less than 0.05 for the regression coefficient (k_2). Furthermore, the value of k_2 is approximately 0.03 for the steering and leading tandem axles in Segment II, and it is around 0.06 for all three axles types in Segment III. One significant difference is that Segment III comprises a higher proportion of AC pavement and a reduced proportion of CCPR material compared with Segment II. This difference in material composition could lead to varying thermal properties and responses to temperature changes.

After obtaining the exponential regression relationships, the total strains recorded were normalized to the reference temperature of 20°C (68°F) using Equation 6. This equation applies a temperature correction factor, calculated from the temperature coefficient of strain (k_2) and the difference between the reference temperature (T_R) and measured temperature (T) (Timm, 2020). Figure 14 and Figure 15 show the temperature-normalized total strain responses for the loading scenarios.

$$\varepsilon_{T_R} = \varepsilon_T \times e^{k_2 \times (T_R - T)} \quad \text{Equation 6}$$

Where:
ε_T = microstrain measured at reference temperature, T_R.

k_1 and k_2 = regression coefficients.
e = exponential constant (2.718282).
T = reference mid-depth pavement temperature.

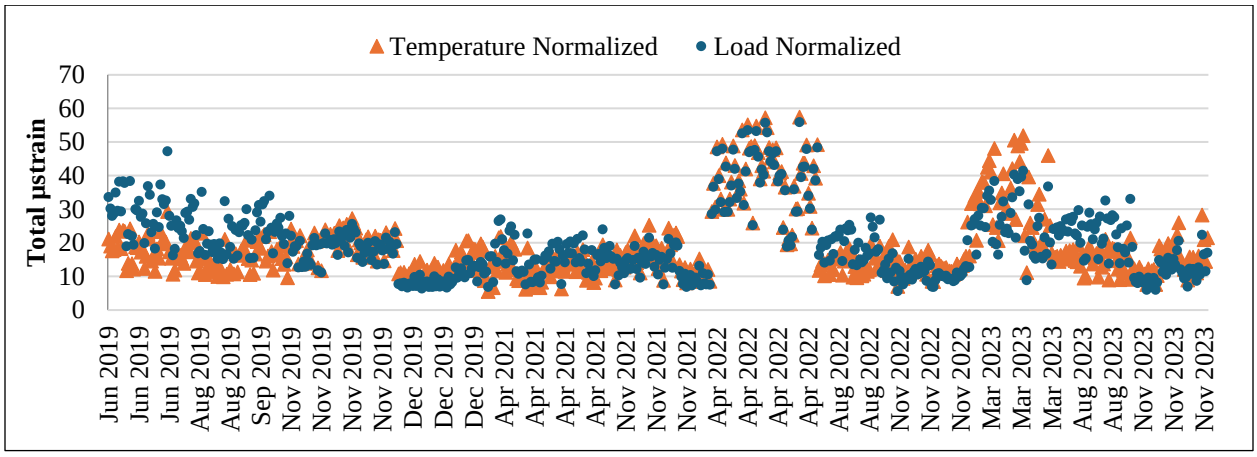

(a)

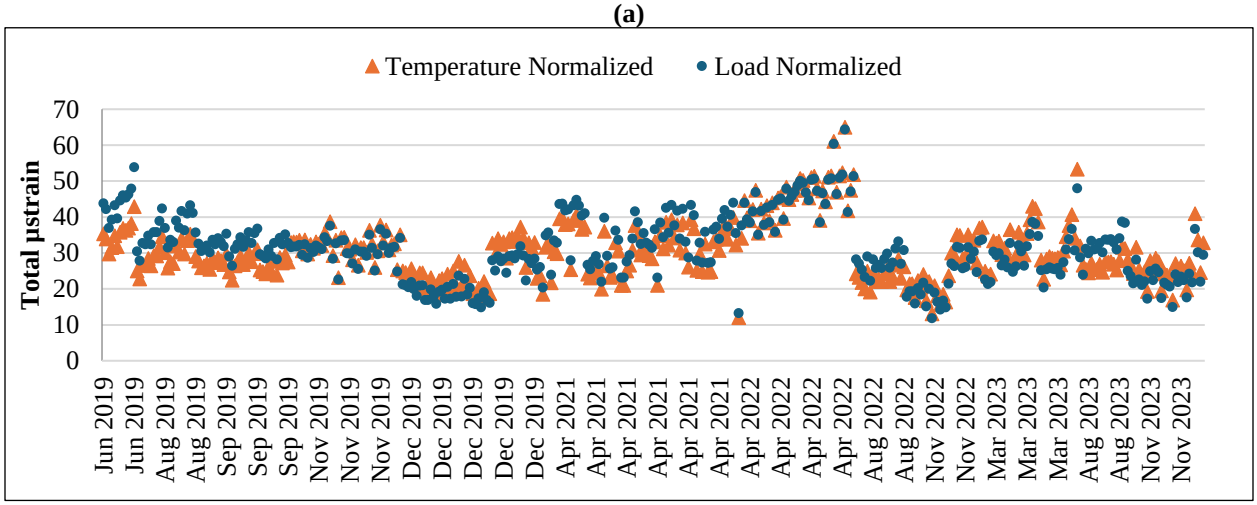

(b)

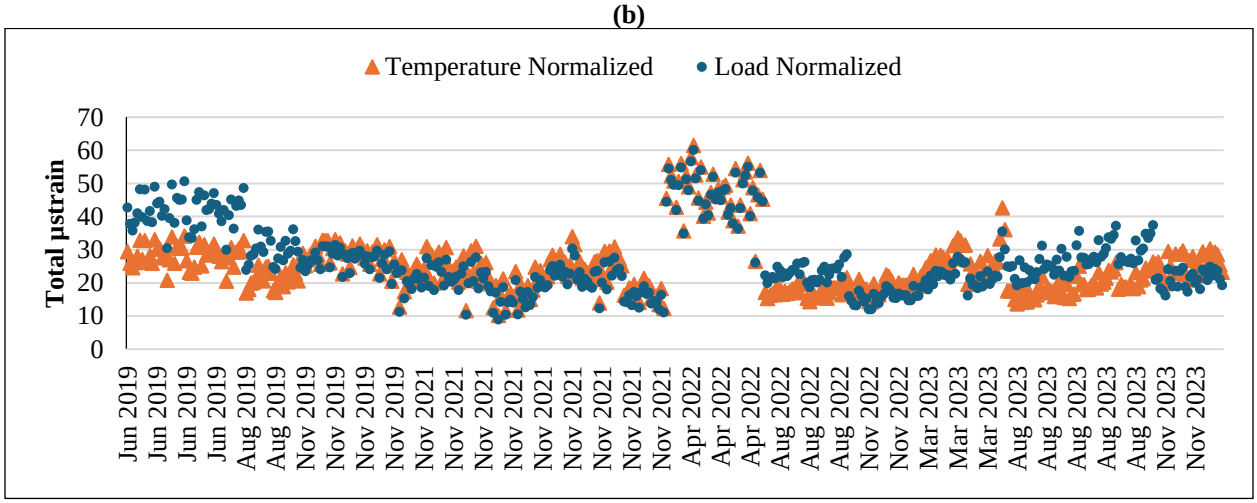

(c)

Figure 14. Load and Temperature-Normalized Total Strain at the Bottom of the Cold Central Plant Recycling Layer to 20°C (68°F) over Time (Segment II): (a) Steering Axle; (b) Single-Dual Tire Axle; (c) Leading Tandem Axle

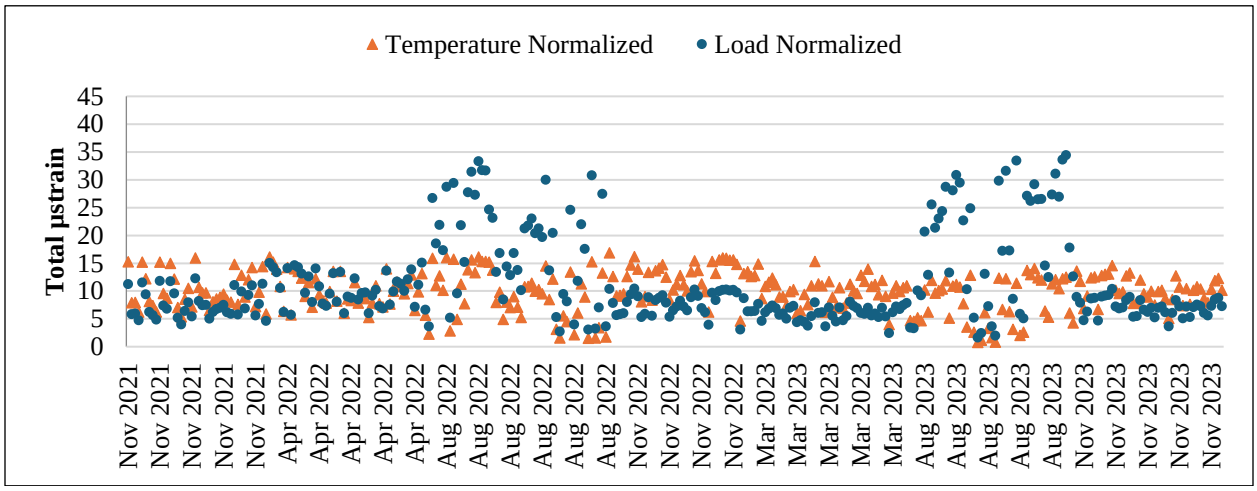

(a)

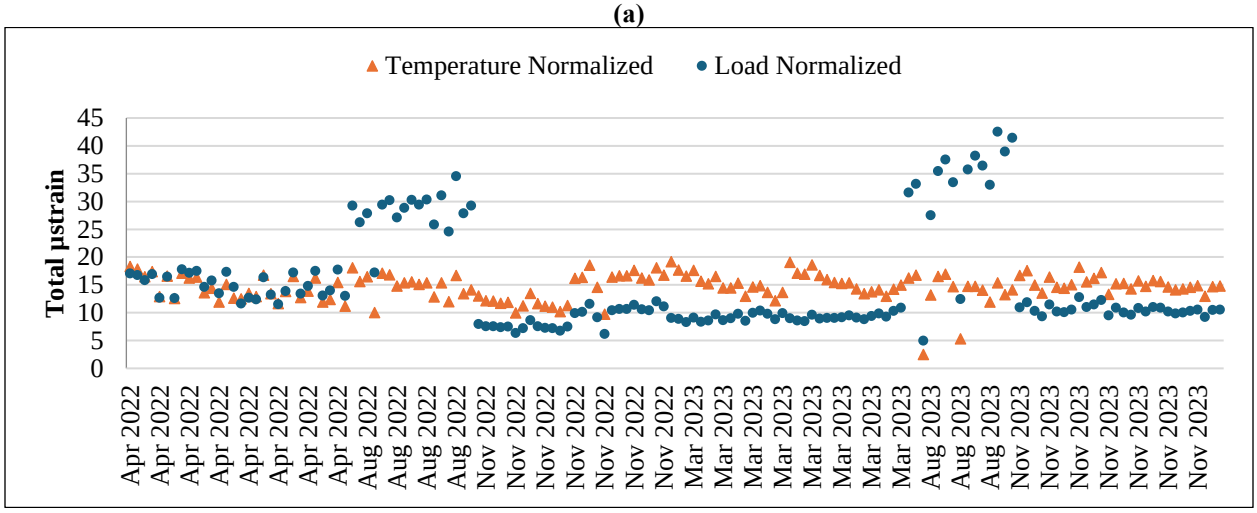

(b)

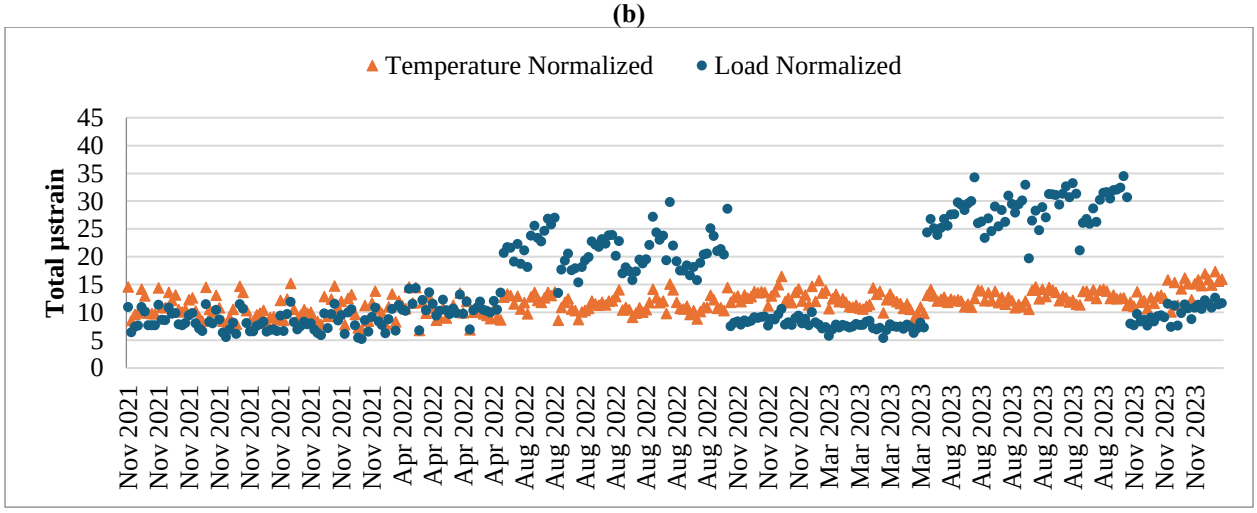

(c)

Figure 15. Load and Temperature-Normalized Total Strain at the Bottom of the Cold Central Plant Recycling Layer to 20°C (68°F) over Time (Segment III): (a) Steering Axle; (b) Single-Dual Tire; (c) Leading Tandem Axle

As mentioned previously, the 95th percentile of the total strain responses was used as a representative value for each field measurement event.

Table **7** summarizes the results. The temperature values reported in

Table **7** are the average mid-depth temperatures during the respective measurement event. To further facilitate data interpretation, the response-normalizing results were categorized based on the seasons in which the tests were conducted. Specifically, the seasons were classified as summer (June–September), fall (October–December), and spring (March–April).

Table 7 shows that the load-normalized measured total strain at the bottom of the CCPR layer is higher in the summer than in the fall. This scenario is expected because the average temperature is higher in the summer than in the fall, and higher temperatures result in higher deformations and strains.

In Segment II, researchers noticed that strain responses decreased over time when examining the load and temperature-normalized total strain for each season. This trend can be attributed to an overall stiffness increase in the pavement layers, especially in the cement-stabilized FDR layer, which is characterized by high initial strength and further strengthened through continued cement hydration (Reeder et al., 2019). In addition, notably high strain responses occur in March and April, when pavement structure bearing capacity may decrease because of elevated moisture content, as documented (National Centers for Environmental Information, 2021). Furthermore, upon temperature normalization, the average longitudinal total strain induced by steering axles (5,300 pounds), single-dual tire axles (9,800 pounds), and leading tandem axles (7,600 pounds) over the section was 26 µstrain, 37 µstrain, and 31 µstrain, respectively.

In Segment III, the average longitudinal total strain after load and temperature normalization generated by the steering, single-dual tire, and leading tandem axles were 15 µstrain, 17 µstrain, and 15 µstrain, respectively. For the steering axle, the strain value for Segment III was 56% of the value measured for Segment II. Meanwhile, for the single-dual tires and leading tandem axles, the strain values were approximately 47% of the value measured for Segment II.

Table 7. Summary of Total Strain at the Bottom of Cold Central Plant Recycling Normalized by Load and Temperature. "Strain load normalized" refers to total strain normalized by load. "Strain temperature normalized" denotes the strain normalized by load and then normalized to a reference temperature of 68°F.

				Steering (5,300 lb)		Single-Dual Tire (9,800 lb)		Leading Tandem Axle (7,600 lb)	
Season	Day	Air Temperature (°C)	Mean Pavement Temperature (°C)	Strain Load Normalized (μstrain)	Strain Temperature Normalized (μstrain)	Strain Load Normalized (μstrain)	Strain Temperature Normalized (μstrain)	Strain Load Normalized (μstrain)	Strain Temperature Normalized (μstrain)
Segment II									
Summer	**Jun-2019**	29.35	33.27	38.33	24.12	50.58	40.53	48.83	33.25
	Aug-2019	27.04	32.07	32.68	21.44	42.32	34.60	35.95	25.34
	Sep-2019	27.73	30.08	31.86	22.40	35.61	30.09		
	Aug-2022	25.06	29.32	25.83	18.66	31.54	27.00	26.69	25.23
	Aug-2023	26.94	32.09	29.60	19.41	38.46	31.43	34.85	24.55
Fall	**Nov-2019**	14.27	18.02	23.37	25.05	35.40	36.59	30.92	32.75
	Dec-2019	5.97	10.75	14.10	19.48	29.30	34.19		
	Nov-2021	21.30	15.82	19.65	22.73			26.69	30.12
	Nov-2022	10.73	13.95	14.98	18.50	32.45	35.90	19.00	22.64
	Nov-2023	13.15	13.15	17.77	22.57	29.93	33.56	24.37	29.72
Spring	**Apr-2021**	23.61	21.94	23.82	22.26	43.33	41.95		
	Apr-2022	17.36	19.29	53.28	54.61	52.25	52.87	54.99	56.13
	Mar-2023	13.33	13.59	39.43	49.32	38.35	42.68	28.78	34.66
Mean				28.05	**26.20**	38.29	**36.78**	33.11	**31.44**
Segment III									
Summer	**Aug-2022**	23.89	30.96	31.56	16.74	31.78	16.83	26.93	14.86
	Aug-2023	30.37	34.94	33.08	13.94	41.77	17.54	32.91	14.63
Fall	**Nov-2021**	20.37	15.28	11.73	15.42			11.35	14.67
	Nov-2022	10.47	12.26	10.26	16.06	11.51	18.05	9.89	15.05
	Nov-2023	14.26	13.64	9.15	13.21	12.11	17.52	11.97	16.90
Spring	**Apr-2022**	19.51	20.56	14.55	14.09	17.62	17.06	13.94	13.53
	Mar-2023	10.69	11.07	7.79	13.06	10.34	17.38	8.17	13.27
Mean				16.87	**14.65**	20.86	**17.40**	16.45	**14.70**

Tensile Strain

Similar to the total strain analysis section, this section focuses on the tensile component of strain. For each testing date and axle type, tensile strain responses, represented by minimum strain values, were identified for each pass of each axle from the testing vehicles. The 95th percentile of these values was also calculated to determine a representative tensile strain for each date. This representative strain was then normalized by load and temperature, following the methodology used for total strain. Table 8 presents the resulting correlation coefficients.

Table 8. Summary of Tensile μstrain and Average Pavement Temperature Relation—Bottom Cold Central Plant Recycling Layer

Axle Type		Regression				
		Observations	k_1	k_2	R-squared	p-value k_2
Segment II	Steering	11	2.89	0.046	0.87	7.2×10^{-5}
	Single-Dual Tire	7	9.22	0.011	0.53	6.1×10^{-2}
	Leading Tandem	7	6.47	0.022	0.72	$1.6 \times 10^{--2}$
Segment III	Steering	7	3.63	0.053	0.95	1.2×10^{-4}
	Single-Dual Tire	6	4.39	0.052	0.99	2.9×10^{-4}
	Leading Tandem	7	3.86	0.051	0.98	1.5×10^{-4}

The exponential regression summary in Table 8 indicates a strong, statistically significant positive correlation between temperature and pavement strain (high R^2, $p < 0.05$ for k_2 in five of six cases). The temperature coefficient (k_2) ranged from 0.02 to 0.05 in Segment II and was around 0.05 in Segment III, similar to the total strain results.

Table 9 shows load and temperature-normalized tensile strains for each field measurement. In Segment II, the tensile strain decreased over time, with March and April peaks consistent with total strain trends. After temperature normalization, average tensile strains were 12 μstrain (steering), 14 μstrain (single-dual tire axle), and 15 μstrain (leading tandem axles), representing approximately 42% of total strain. In Segment III, average tensile strains were 10 μstrain (steering), 12 μstrain (single-dual tire axle), and 11 μstrain (leading tandem axles), accounting for 72% of total strain. Tensile strain values were more consistent between segments, with Segment II exhibiting slightly higher strains (approximately 2 μstrain difference).

Table 9. Summary of Tensile Strain at the Bottom of Cold Central Plant Recycling Normalized by Load and Temperature. "Strain load normalized" refers to total strain normalized by load. "Strain temperature normalized" denotes the strain normalized by load and then normalized to a reference temperature of 68°F.

				Steering (5,300 lb)		Single-Dual Tire (9,800 lb)		Leading Tandem Axle (7,600 lb)	
Season	Day	Air Temperature (°C)	Mean Pavement Temperature (°C)	Strain Load Normalized (µstrain)	Strain Temperature Normalized (µstrain)	Strain Load Normalized (µstrain)	Strain Temperature Normalized (µstrain)	Strain Load Normalized (µstrain)	Strain Temperature Normalized (µstrain)
Segment II									
Summer	**Jun-2019**	29.35	33.27	13.59	7.38	14.93	12.95	15.29	11.36
	Aug-2019	27.04	32.07	12.39	7.11	11.63	10.22	12.72	9.71
	Sep-2019	27.73	30.08	13.84	8.70	11.94	10.72		
	Aug-2022	25.06	29.32	10.88	7.08	8.44	7.64	9.97	8.09
	Aug-2023	26.94	32.09	11.63	6.66	10.22	8.98	14.12	10.76
Fall	**Nov-2019**	14.27	18.02	8.54	9.36	12.07	12.33	13.90	14.53
	Dec-2019	5.97	10.75	4.85	7.43	10.92	12.05		
	Nov-2021	21.30	15.82	5.94	7.20			9.11	10.00
	Nov-2022	10.73	13.95	5.20	6.87	10.76	11.48	8.36	9.57
	Nov-2023	13.15	13.15	5.58	7.65	9.46	10.18	9.98	11.63
Spring	**Apr-2021**	23.61	21.94	5.16	4.72	7.24	7.10		
	Apr-2022	17.36	19.29	26.18	27.05	28.39	28.61	29.40	29.87
	Mar-2023	13.33	13.59	34.15	45.89	32.13	34.41	26.75	30.89
Mean				12.15	**11.78**	14.01	**13.89**	14.96	**14.64**
Tensile/Total Strain (%)				43%	**45%**	37%	**38%**	45%	**47%**
Segment III									
Summer	**Aug-2022**	23.89	30.96	21.45	11.99	21.61	12.24	18.53	10.62
	Aug-2023	30.37	34.94	21.57	9.76	27.24	12.55	23.05	10.79
Fall	**Nov-2021**	20.37	15.28	8.26	10.61			8.18	10.39
	Nov-2022	10.47	12.26	7.81	11.78	9.34	13.96	8.05	11.93
	Nov-2023	14.26	13.64	7.31	10.25	9.73	13.53	8.97	12.39
Spring	**Apr-2022**	19.51	20.56	9.69	9.40	11.46	11.14	9.43	9.17
	Mar-2023	10.69	11.07	5.56	8.93	7.25	11.53	6.34	9.99
Mean				11.66	**10.39**	14.44	**12.49**	11.79	**10.75**
Tensile/Total Strain (%)				69%	**71%**	69%	**72%**	72%	**73%**

Figure 16 and Figure **17** present the total and tensile strains as a function of ESALs, respectively. This analysis considered steering and single dual-tire configurations. Appendix F provides further detailed calculations related to traffic.

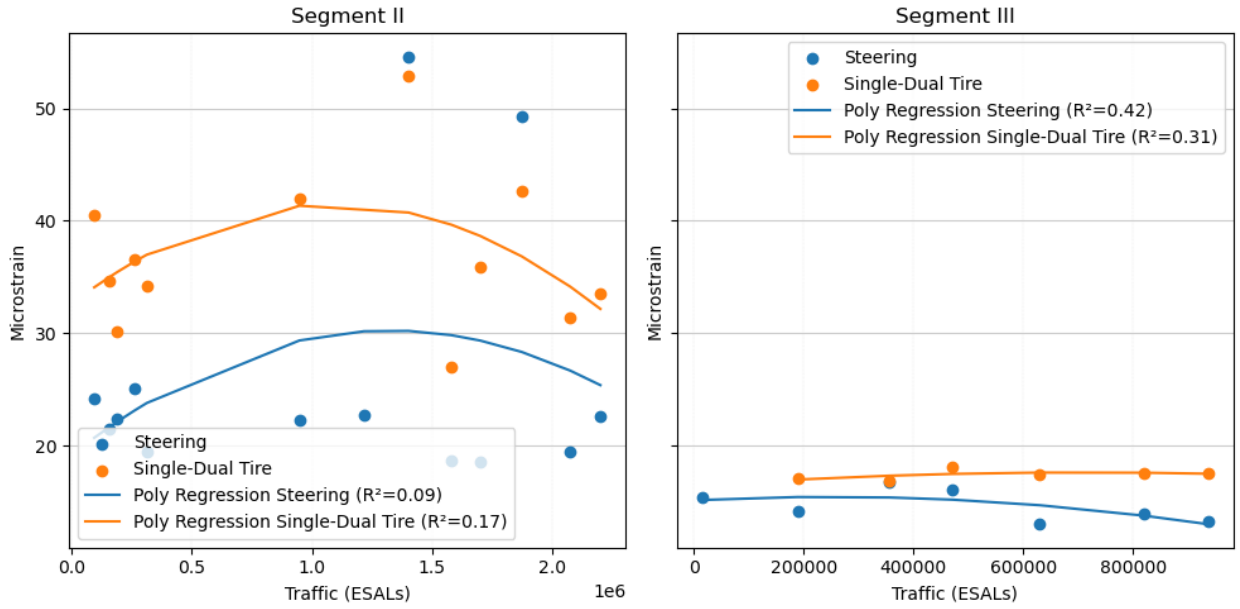

Figure 16. Total Strain Measured at the Bottom of Cold Central Plant Recycling Layer as a Function of Traffic (ESALs) for Steering and Single Dual-Tire Configurations. ESALs = equivalent single-axle loads.

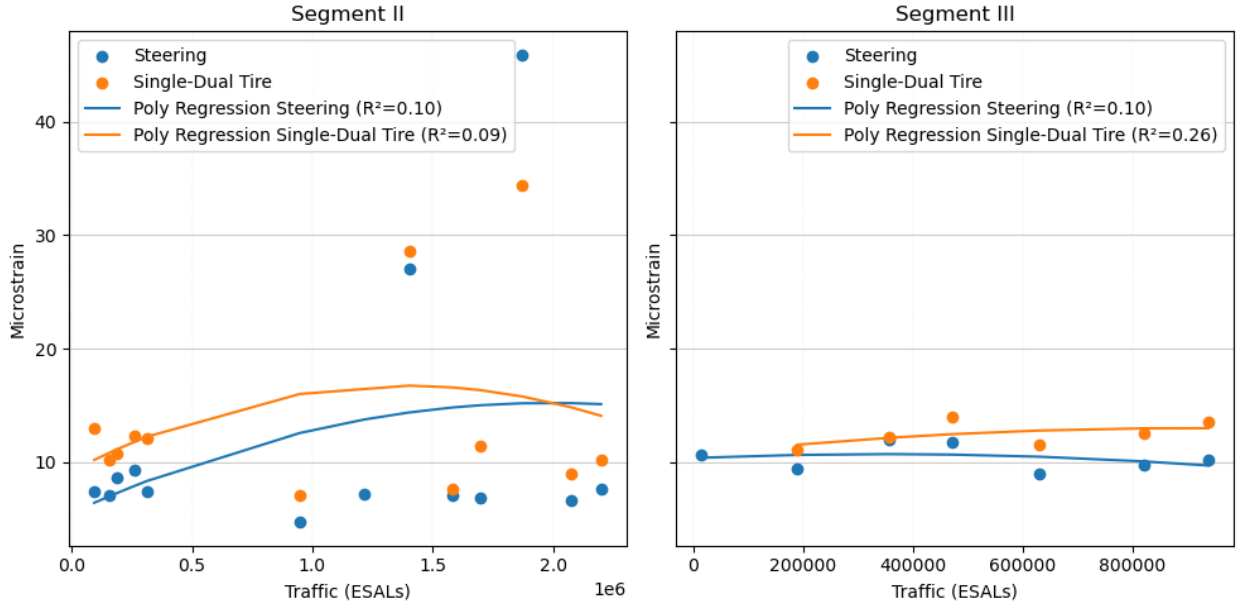

Figure 17**. Tensile Strain Measured at the Bottom of Cold Central Plant Recycling Layer as a Function of Traffic (ESALs) for Steering and Single Dual-Tire Configurations. ESALs = equivalent single-axle loads.**

In Figure 16 and Figure **17**, Segment II shows a trend of initial strain increase followed by a decrease with traffic accumulation, followed again by periodic increases. The R^2 values of the regression equation are relatively low, indicating a weak fit for the polynomial regression. On

the other hand, Segment III exhibits more stable or gradual trends within the analyzed traffic ranges and is a better fit than Segment II.

Stress

During the construction of Segment II, one of the pressure cells at the bottom of the CCPR layer was damaged. In addition, stress responses from the remaining five cells were not recorded between September 2019 and November 2020 because of a software compatibility issue, which was subsequently resolved.

The 95th percentile of the normalized stress responses obtained for each axle type was also normalized to a reference load, and temperature corrected to compare the responses from different dates (Appendix G). This procedure is similar to the one used for strain responses. Equation 7 and Table 10 present the correlation equation terms and the coefficient of correlation obtained, respectively.

$$\sigma_T = k_1 \times e^{T \times k_2} \quad \text{Equation 7}$$

Where:
σ_T = stress measured at temperature, T.
k_1 and k_2 = regression coefficients.
e = exponential constant (2.718282).
T = mid-depth pavement temperature.

Table 10. Summary of Stress and Average Pavement Temperature Relationship

		Stress Bottom CCPR					Stress Top Subgrade				
		Observations	k_1	k_2	R^2	p-value k_2	Observations	k_1	k_2	R^2	p-value k_2
Segment II[a]	Steering	8	13.82	0.023	0.90	2.1×10^{-4}	7	1.61	0.012	0.85	2.5×10^{-3}
	Single-Dual Tire	8	15.95	0.018	0.73	1.1×10^{-4}	6	3.12	0.007	0.61	5.4×10^{-2}
	Leading Tandem	9	16.25	0.014	0.39	7.6×10^{-2}	7	2.45	0.013	0.84	4.3×10^{-3}
Segment III[b]	Steering	-	-	-	-		7	1.10	0.029	0.67	4.1×10^{-2}
	Single-Dual Tire	-	-	-	-		6	2.27	0.023	0.74	4.3×10^{-2}
	Leading Tandem	-	-	-	-		7	1.81	0.028	0.83	7.4×10^{-3}

CCPR = cold central plant recycling. [a] For Segment II, stresses were measured at the bottom of the CCPR layer and at the top of the subgrade. [b] For Segment III, stresses were measured at the top of the subgrade only.

The Table 10 regression summary shows a strong positive relationship between temperature and stress responses, evidenced by high R^2 values (exceeding 0.6 in 8 out of 9 regressions), and a statistically significant influence of temperature, based on the p-values less than 0.05 for the regression coefficient (k_2). Moreover, the value of k_2 is approximately 0.02 for the stress values recorded at the bottom of the CCPR layer in Segment II and at the top of the

subgrade in Segment III. However, for the stresses at the top of the subgrade in Segment II, the k_2 value is lower, regressed as less than 0.013. Similar to the strain data, stress responses were normalized to 20°C (68°F) for meaningful comparisons. Table 11 summarizes the temperature-normalized stress responses.

Table 11. Temperature Corrected Stress in psi

Segment	Date	Steering		Single-Dual Tire		Leading Tandem	
		CCPR[a]	Subgrade[b]	CCPR	Subgrade	CCPR	Subgrade
II	**June 2019**	21.59	2.08	23.31	3.41	20.74	3.13
	August 2019	19.70	1.95	20.40	3.47	19.46	3.10
	November 2021		2.08			23.73	3.38
	April 2021	20.37	1.96	24.70	3.56	20.82	2.96
	August 2022	22.95	2.18	23.11	3.83	24.23	3.34
	November 2022	20.65		18.21		16.31	
	March 2023	22.82	2.04	22.13	3.51	16.68	3.07
	August 2023	23.30	1.98	23.85	3.63	22.51	3.32
	November 2023	22.59		26.14		26.47	7.95
	Average	**21.75**	**2.04**	**22.73**	**3.57**	**21.22**	**3.78**
III[c]	**November 2021**		1.47				2.90
	April 2022		2.42		3.86		3.21
	August 2022		1.64		3.17		2.78
	November 2022		1.56		2.85		2.95
	March 2023		2.62		4.44		4.02
	August 2023		2.11		3.85		3.41
	November 2023		1.85		3.41		2.89
	Average		**1.95**		**3.60**		**3.17**

CCPR = cold central plant recycling. [a] CCPR refers to the stress responses measured at the bottom of the CCPR layer. [b] Subgrade refers to the stresses at the top of the subgrade. [c] For Segment III, stresses were measured at the top of the subgrade only.

In Segment II, the average normalized stress response at the bottom of the CCPR for steering axle, single-dual tire axle, and leading tandem axles was 21.7, 22.7, and 21.2 psi, respectively. Regarding the stresses measured at the top of the subgrade, the average adjusted values were 2.0, 3.6, and 3.2 psi for steering, single-dual tire, and leading tandem axles, respectively.

The Boussinesq theory of a point load applied on the surface of an infinitely large half space was utilized to assess the stress responses recorded during the tests. Using the average load for response normalization, vertical stresses were calculated at depths of 10 and 24 inches, corresponding to the pressure cells' locations. The calculated stresses were 25, 47, and 36 psi at the bottom of the CCPR layer and 4.4, 8.1, and 6.3 psi at the top of the subgrade for steering, single-dual tire, and leading tandem axles, respectively. These calculated stresses are higher than the measured values, and the ratio of pressure responses between the cells at the bottom of the CCPR layer and those at the top of the subgrade indicates a more favorable load distribution—10 to 16% compared with the 17% calculated distribution between these two depths.

In Segment III, the average temperature-normalized stress response at the top of the subgrade for steering axle, single-dual tire axle, and leading tandem axles was 2.0, 3.6, and 3.2 psi, respectively. These values are similar to those recorded in Segment II.

Linear Elastic Validation

The measured total and tensile strain responses and material properties used to characterize the pavement structures were verified through modeling in the layered elastic software (OpenPave, 2025). This analysis focused on the responses from two-axle trucks, the predominant vehicle type used in most field measurement events. The determination of the modulus values for stone matrix asphalt, CCPR, and OGDL was achieved through analysis of the master curve. The relationship is expressed mathematically as:

$$\log E = \delta + \frac{\alpha}{1+e^{\beta+\gamma(logt-C(log\eta-log\eta_{ref}))}} \quad \text{Equation 8}$$

Where:
E = dynamic modulus (psi).
α, β, γ, δ, C = adjustment parameters.
t = loading time (seconds), Brown equation = $\log(t) = 0.5d - 0.2 - 0.94\log(v)$.
η = viscosity (cPoise), $\log(log\,\eta) = A + VTS(logT_R)$.
η_{ref} = viscosity at reference temperature (cPoise), $\log(log\eta_{ref}) = A + VTS(log(T_R)_0)$.
T_R = temperature (°Rankine).
$(T_R)_0$ = reference temperature (°Rankine).
A = regression intercept of viscosity temperature susceptibility equation.
VTS = regression slope of viscosity temperature susceptibility equation.
v = vehicle speed (km/h).

The strain responses were normalized to a pavement temperature of 68°F. Table 12 outlines the procedural steps and calculations involved in determining the modulus.

Table 12. Calculations for Determining Modulus Using the Sigmoidal Master Curve

Parameter	Variables	SMA	CCPR	OGDL
Master Curve Fitting Parameters	α	2.99520	2.34381	2.09207
	β	– 0.88682	– 1.69682	– 0.28307
	γ	0.35357	0.31611	0.40078
	δ	3.74119	3.63271	4.16864
	C	1.20204	1.01884	1.16486
Binder Characteristics	A	9.93	10.98	10.98
	VTS	– 3.29	– 3.68	– 3.68
	$(T_R)_0$ Fahrenheit	70.00	70.00	70.00
	$(T_R)_0$ Rankine	529.67	529.67	529.67
Loading Time	log (t) time of loading at the temperature of interest	– 2.005	– 1.941	– 1.890
	Frequency (Hz) 1/(2πt)	16.1	13.9	12.4
	log t = log (1/F)	– 1.207	– 1.143	– 1.092
Modulus	T_R Fahrenheit	**68**	**68**	**68**

Parameter	Variables	SMA	CCPR	OGDL
	T_R Rankine	527.670	527.670	527.670
	log η_{ref}	9.476	9.029	9.029
	log η	9.595	9.156	9.156
	E* (psi)	1,338,135	525,502	400,963

CCPR = cold central plant recycling; OGDL = open-graded drainage layer; SMA = stone matrix asphalt; VTS = viscosity temperature susceptibility.

Table 13 presents the pavement structure utilized in the modeling process, detailing the characteristics of each layer. It includes each segment's modulus, Poisson's ratio, and thickness. For this linear elastic validation, calculations were performed using two different scenarios for the resilient modulus of the FDR layer, as presented in the *AASHTOWare Pavement ME User Manual* (VDOT, 2017). One scenario assumes a resilient modulus of 80,000 psi, which is close to the estimated modulus for FDR as a non-stabilized base layer. In contrast, the other scenario assumes a resilient modulus of 750,000 psi, representing the estimated modulus for cement-treated FDR as a chemically stabilized layer.

Table 13. Pavement Structure Used for Modeling

Layer	Segment II Thickness (in)	Segment III Thickness (in)	Poisson's Ratio	Modulus (psi)
SMA	4	4.5	0.35	1,338,000
CCPR	6	5	0.35	526,000
OGDL	2	2	0.35	401,000
FDR	12	12	0.20	80,000 and 750,000
Subgrade			0.40	12,300

CCPR = cold central plant recycling; FDR = full-depth reclamation: OGDL = open-graded drainage layer; SMA = stone matrix asphalt.

In the *Mechanistic-Empirical Design Manual* (Hossain, 2010), pavement performance concerning bottom-up fatigue cracking is characterized by evaluating the tensile strain at the bottom of the asphalt layer. As such, the evaluation point for this purpose should ideally be at the bottom of OGDL. However, during the construction of the pavement section, strain gauges were installed at the bottom of the CCPR layer instead for construction reasons because the thickness of OGDL was only slightly thicker than the gauges.

Table 14. provides a summary of the average total and tensile strain measured using the strain gauges and the values calculated with OpenPave for both segments, resulting from steering and single-dual tire axle configurations. For the steering axle, a half axle load of 5,300 pounds was used, and for the single-dual tire axle, a half axle load of 9,800 pounds was used. This half axle load consisted of two tires, each carrying 4,900 pounds. In addition, a tire pressure of 750 kPa was assumed. In terms of the point analysis, the longitudinal strain was modeled at the bottom of the CCPR layer under the wheel for the steering axle, whereas strain was modeled both under the wheel and between the two wheels for the single-dual tire axle. These results were compared with the strain measured by gauges.

Table 14. Comparison of Measured and Calculated Tensile Strain

Segment	Axle	CCPR Measured Tensile Strain (με)	Modeled Location	Calculated Strain Using OpenPave			
				Case FDR 1[c]	Case FDR 2[d]	Case FDR 1	Case FDR 2
				CCPR (με)	CCPR (με)	OGDL (με)	OGDL (με)
II	**Steering**	**12**	UW[a]	27.2	12.1	34.5	5.1
	Single-Dual Tire	**14**	BW[b]	39.5	13.6	51.8	6.4
III	**Steering**	**10**	UW	28.4	12.9	36.1	5.3
	Single-Dual Tire	**12**	BW	40.7	14.0	53.7	6.5

CCPR= cold central plant recycling; FDR = full-depth reclamation; OGDL = open-graded drainage layer. [a] UW denotes evaluation point under the wheels. [b] BW stands for evaluation point between the wheels. [c] Case FDR 1 corresponds to a pavement structure with an FDR layer that has a resilient modulus of 80,000 psi. [d] Case FDR 2 refers to a pavement structure with an FDR layer that has a resilient modulus of 750,000 psi.

The results in

Table 14. show that the average tensile strains, recorded by the instrumentation at the bottom of the CCPR layer, are generally close to the values calculated using the case FDR 2 (750,000 psi FDR modulus) for both segments. In Segment II, the difference is approximately 0.1 µstrain for the steering axle and 0.4 µstrain for the dual axle (less than 3% for both cases). However, Segment III exhibits a larger difference (~3 µstrain for steering axle) between measured and modeled strains compared with Segment II. Figure 18 shows a seasonal comparison of the tensile strain responses for steering axle (left subplot) and single-dual tire axle (right subplot) for both segments.

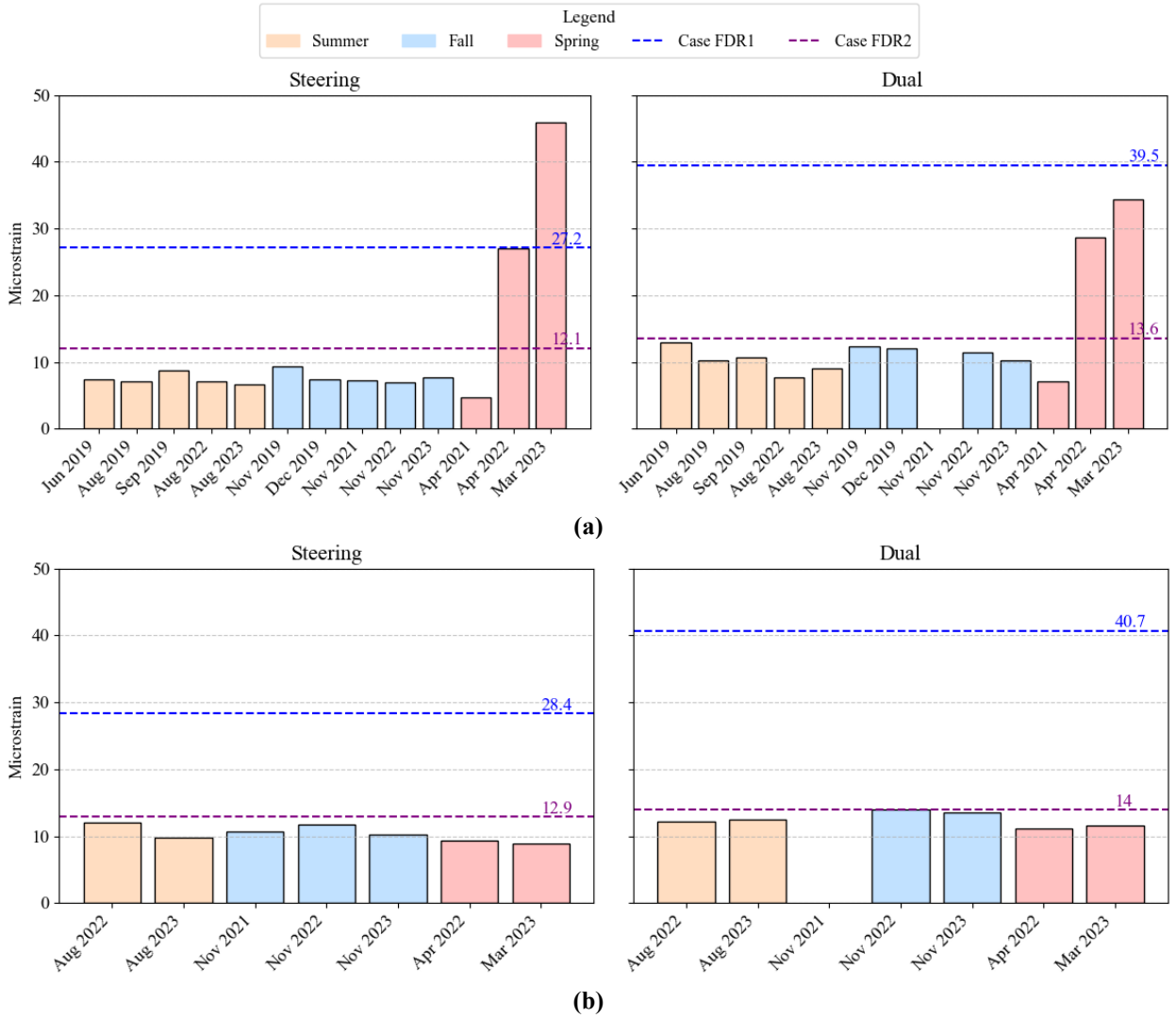

Figure 18. Seasonal Comparison of Tensile Strain Responses for Steering Axle and Single-Dual Tire Axle: (a) Segment II; (b) Segment III. The left subplot shows the steering strain data, and the right subplot shows the dual strain data across summer, fall, and spring. Two reference lines are added for comparison: Case FDR 1 and case FDR 2. Seasonal variations are color coded for clarity. FDR = full-depth reclamation.

For Segment II, tensile strain values remain relatively consistent across summer and fall (after temperature normalizing) for both types of trucks. However, a significant increase is observed during the spring, with the highest values recorded in April 2022 and March 2023. Both case FDR 1 and case FDR 2 reference lines indicate that spring values for the steering axle

and single-dual tire axleexceed the reference lines. In contrast, the values in the summer and fall stay closer to or below these reference lines. For Segment III, all strain responses for both axle types remain near the case FDR 2 reference line.

In terms of the calculated strain at the bottom of OGDL, it remained below the very conservative endurance limit of 70 μstrain in both segments and under both cases (FDR 1 and FDR 2), ensuring sufficient pavement stiffness to prevent bottom-up fatigue cracking (Tran et al., 2016). This scenario assumes that the endurance limits in Table 15 apply to an OGDL-type material. Table 15 presents additional endurance strain limits.

Table 15. Endurance Strain Limits per Author (Adapted from Tran et al., 2016)

Author	Value (με)	Comments
Monismith and McLean (1972)	70	First value for bituminous mixes
Maupin and Freeman (1976)	70	
Nishizawa et al. (1997)	200	In-service pavements in Japan
Wu et al. (2004)	96 and 158	Determined from backcalculated stiffness data
Thompson and Carpenter (2006)	70 to 100	Practical range
Yang et al. (2006)	125	Pavement design in China
Von Quintus (2006)	65	
Prowell et al. (2010)	75 to 200	Laboratory testing data
Carpenter and Shen (2009)	90 to 300	University of Illinois
Willis and Timm (2009)	100	NCAT Pavement Test Track

NCAT = National Center for Asphalt Technology.

Traffic Speed Deflectometer Analysis

Traffic speed deflectometer (TSD) measurements were conducted for Segments II and III 1 year after opening to traffic. This timeframe allows an assessment of early-stage pavement performance. Table 16 summarizes environmental and operational data (air and surface temperatures, speed, and load). The analysis evaluated the structural response of the pavement by considering the maximum deflection (D0), deflection bowl shape, and the bearing capacity of the upper and lower pavement layers based on the surface curvature indices SCI12 and SCIsub.

Table 16. Environmental and Operational Data Summary

Segment	Date	Statistic	Air Temperature (°F)	Surface Temperature (°F)	Speed (mph)	Load (lb)
II	09/14/2020	Mean	82.0	82.7	53.1	10,065.5
		Standard Deviation	0.1	0.8	0.7	126.5
III	10/16/2022	Mean	75.7	68.7	63.4	10,152.8
		Standard Deviation	0.1	0.9	0.6	129.1

Figure 19 shows D0 for all Segments II and III projects. Both graphs show relatively low deflection values and some variability in D0 values along the segment, with localized peaks indicating areas of higher deflection. Segment II exhibits both a slightly higher average D0 and greater variability compared with Segment III. However, the two projects perform similarly from a deflection perspective. Segment III has a thicker pavement section and includes the stabilized subgrade in the existing lanes (where the TSD data were collected), which may have contributed to the slightly lower deflection values. In addition, Segment II was tested at a time of higher average air temperature. Figure 19 also shows that Segment II had increased deflections near the instrumentation location.

Figure 20 shows the SCI12 and SCIsubgrade, which indicate structural properties of the upper portions of the pavement and foundation layers, respectively. Although both segments exhibit similar overall stiffness in the upper pavement layers and subgrade, Segment II shows a noticeable peak in SCI12 close to and surrounding the instrumentation location, but this peak was not observed for the SCIsubgrade. This result shows that the bound pavement layers are less stiff in this area than the rest of the Segment II project. The research team reviewed photographs taken during construction and instrumentation and confirmed that cement was added to the FDR layer during construction of this portion of Segment II. The research team does not believe this result is due to the instrumentation because the area around the instrumentation is similar. In addition, the same installation and construction techniques were used on both Segments II and III.

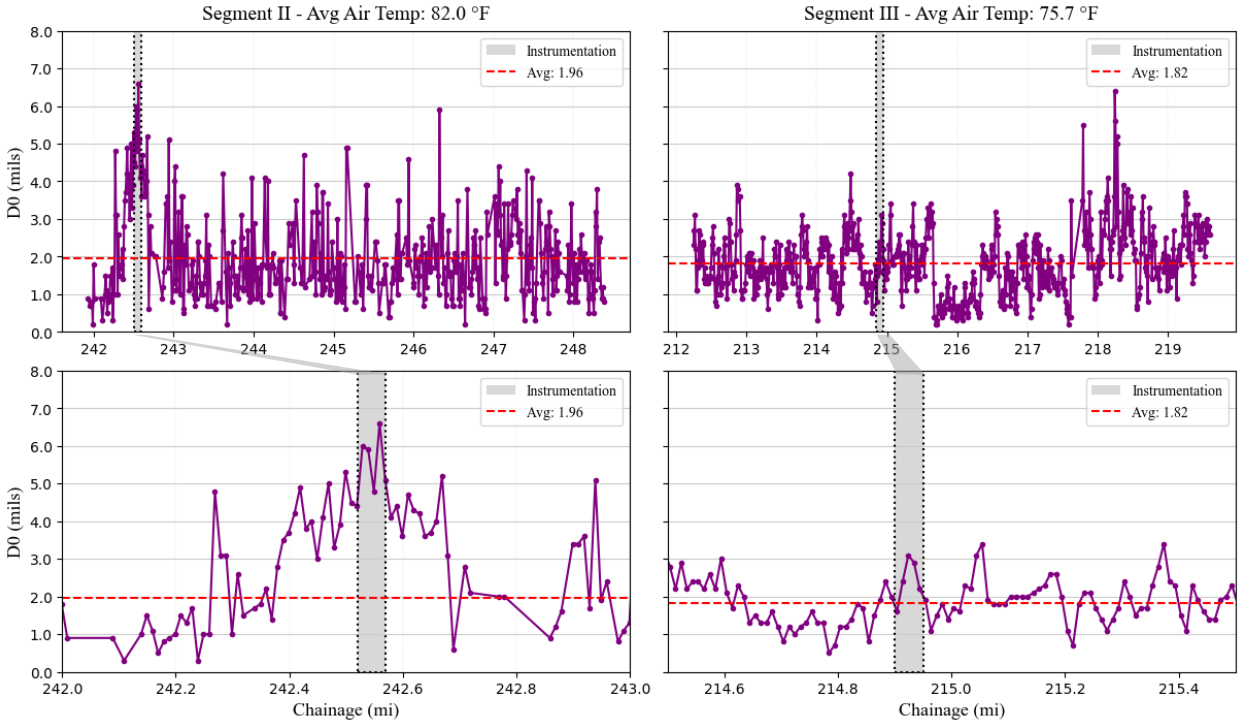

Figure 19. Maximum Deflection Analysis. Gray areas indicate instrumentation locations within each segment. The top row shows the full chainage range for Segments II and III, and the bottom row provides a zoomed-in view focusing on the instrumentation locations within each segment. D0 = maximum deflection.

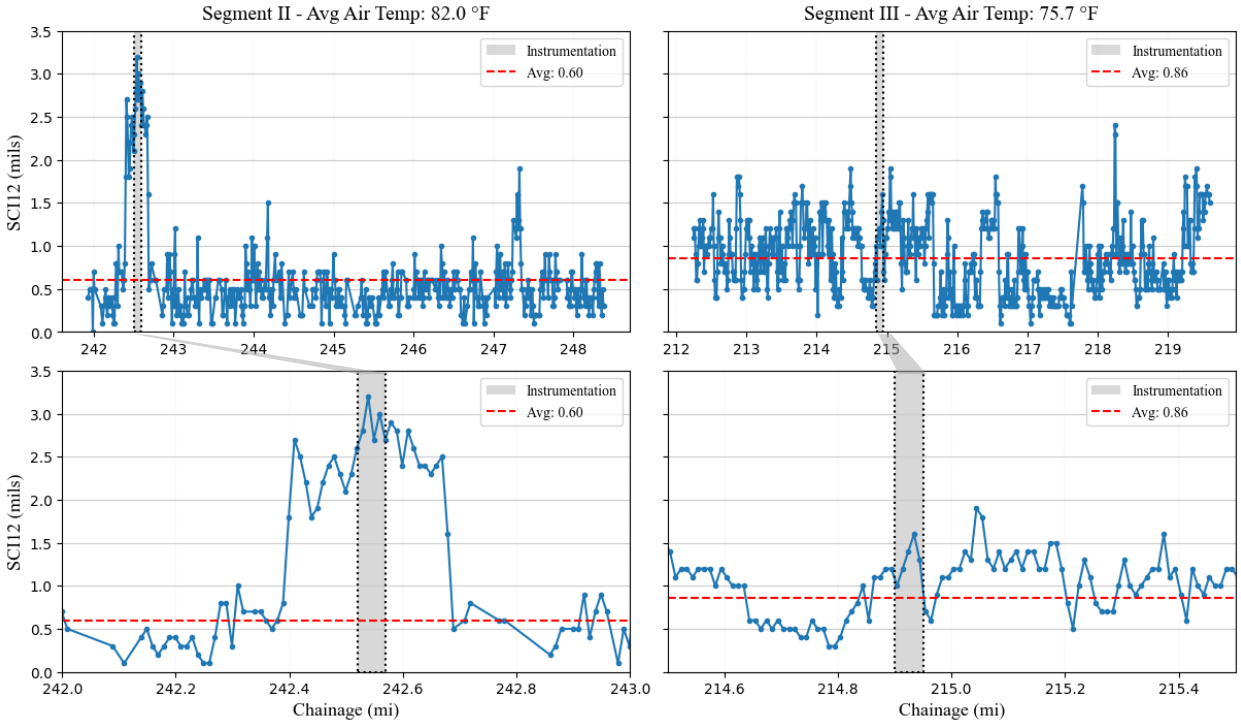

(a)

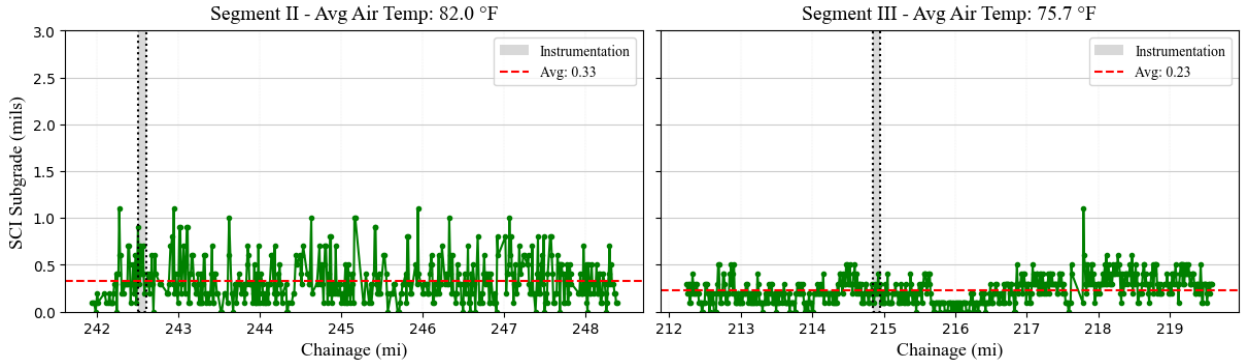

(b)

Figure 20. Structural Condition Index Analysis: (a) SCI12—The Top Row Shows the Full Chainage Range for Segments II and III, and the Bottom Row Provides a Zoomed-in View Focusing on the Instrumentation Locations within Each Segment; (b) SCI Subgrade. SCI = surface curvature indices.

Given the relatively higher deflection values in Segment II near the instrumentation location, the deflection bowls from Segments II and III were analyzed for the segment as a whole and separately for the measurements near the instrumentation (Figure 21). The deflection bowl analysis indicates that Segment II exhibits negligibly higher deflections than Segment III overall. However, a more pronounced difference is observed when examining the measurements near the instrumentation location. Specifically, Segment II shows higher deflections at D0 and lower deflections at D72. This observation supports the results from the validation for total strain, in which FDR moduli for Segment II were lower than those for Segment III.

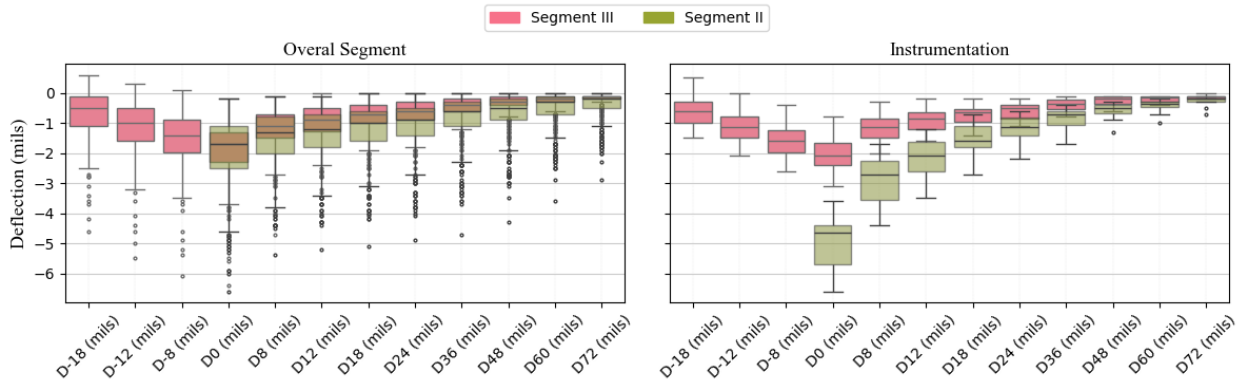

Figure 21. Deflection Bowl Comparison (Left) Overall Segment (Right) near Instrumentation Location. Dx indicates the deflection (mils) at a distance of x from the applied load. The box in the diagram represents the dataset's quartiles, and the whiskers capture the rest of the distribution, except for points classified as outliers based on an Interquartile Range method.

SUMMARY OF FINDINGS

- Pavement response measurements were conducted during the spring, summer, and fall for Segments II and III and during the winter for Segment II. The recorded pavement temperatures adequately represented the expected temporal distribution of pavement temperatures over the study period for each segment.

- Temperature influenced the measured pavement stress and strain responses for Segments II and III.

- All strain gauges, moisture sensors, and thermocouples were functional after construction and remained so for 5 years (Segment II) and 2 years (Segment III). One pressure cell in Segment II became nonfunctional after construction. All three pressure cells installed in Segment III remained fully functional after construction.

- In Segment II, the moisture contents measured at their respective depths remained relatively constant during the initial 3 years of testing. In Segment III, the moisture contents measured at their respective depths remained relatively constant during their 2-year measurement period.

- The load and temperature-normalized total strain values in both segments slightly decreased over the measurement period—5 years for Segment II and 2 years for Segment III.

- The strain response in Segment II was relatively higher during the spring months compared with the rest of the year.

- The strain response in Segment III was more sensitive to temperature changes than Segment II.

- Following load and temperature normalization, the average longitudinal *total* strain in Segment II was approximately 26, 37, and 31 μstrain for the steering axle, single-dual tire axle, and leading tandem axle, respectively. In Segment III, the corresponding normalized average longitudinal total strains were approximately 15, 17, and 15 μstrain, respectively. The total strain values observed in Segment III were approximately one-half of those observed in Segment II.

- Following load and temperature normalization, the average longitudinal *tensile* strain in Segment II was approximately 12, 14, and 15 μstrain for the steering axle, single-dual tire axle, and leading tandem axle, respectively. In Segment III, the corresponding normalized average longitudinal tensile strains were approximately 10, 12, and 11 μstrain, respectively. The tensile strain values observed in Segments II and III were approximately 42 and 72 % of the total strain, respectively.

- The measured strain responses from Segments II and III were much lower than the endurance strain limits reported in the literature.

- Following load and temperature normalization, the average stress at the bottom of the CCPR layer in Segment II was 21.8, 22.7, and 21.2 psi for the steering axle, single-dual tire axle, and leading tandem axle, respectively. No stress measurements were collected at the bottom of the CCPR layer in Segment III.

- Following load and temperature normalization, the average stress at the top of the subgrade in Segment II was 2.0, 3.6, and 3.8 psi for the steering axle, single-dual tire, and leading

tandem axle, respectively. In Segment III, the corresponding average stresses on top of the subgrade were 2.0, 3.6, and 3.2 psi, respectively. Stress responses in Segment II at the top of the subgrade were approximately 10 to 16% of those at the bottom of the CCPR layer.

- When comparing measured versus calculated tensile strains based on a modeling effort employing linear elastic assumptions, the measured tensile strain at the bottom of the CCPR layer in both segments compares well with the calculated tensile strain at the bottom of the CCPR layer assuming a FDR resilient modulus of 750,000 psi.

- Deflection testing results from TSD analysis showed that D0 and SCI12 were higher near the instrumented area in Segment II compared with the rest of the segment. Similar measurements from Segment III did not show this difference. Average deflection values were approximately 2.0 and 1.8 mils for Segments II and III, respectively. Researchers found no differences in the SCIsubgrade near the instrumented section in either segment.

CONCLUSIONS

- *Constructing an experimental test section with embedded pavement instrumentation is an effective means for better understanding pavement structural behavior.*

- *The instrumentation in Segments II and III is likely to provide additional performance information if further data are collected*. These two test sections are likely the only non-test track instrumented pavement recycling test sections in the United States.

- *The moisture content increase in Segment II after November 2022 is attributed to either a change in sensor performance or a reduction in the performance of OGDL*.

- *The increase in strain in Segment II during the spring months was possibly caused by higher moisture contents in the foundation layers*.

- *It is unclear if changes in construction during the instrumentation process were responsible for the increased deflection response measured by TSD analysis within the instrumented area of Segment II*. A similar process was followed for Segment III, and no increase in the deflection response was observed.

- *The TSD deflection and structural modeling results suggest that the FDR layer within the instrumented section of Segment II had a lower stiffness than expected*.

- *Based on the low strain, pressure, and deflection results, the pavement structure used in Segments II and III likely could have been further optimized without negatively affecting the long-term performance*

- *Segments II and III are expected to have a long structural life given their low total and tensile strain, stress, and deflection results. This conclusion is supported by positive*

performance experiences from similar pavement structures placed on I-81 in 2011 and the NCAT Test Track in 2012.

RECOMMENDATIONS

1. *VDOT's Materials Division and VTRC should submit a Research Needs Statement to the Pavement Research Advisory Committee to collect additional response data from the instrumented test sections within Segments II and III. Additional response data should be collected until the sensors are no longer functional*. This work will help support the conclusion of long-life performance. In addition, VTRC should collect performance data from VDOT's pavement management system to confirm the long-life performance of the test section.

2. *VDOT's Materials Division and VTRC should submit a Research Needs Statement to the Pavement Research Advisory Committee to investigate if the design of similar recycled pavement sections (i.e., consisting of asphalt layers, CCPR, and FDR) can be further optimized*.

3. *Based on the information in this study and from other VTRC research, including I-81 and NCAT, VDOT's District Materials and Maintenance staff should consider similar design approaches, such as recycled materials with a stabilized foundation, as those used in this study when existing pavements require deep repair or reconstruction*.

IMPLEMENTATION AND BENEFITS

Researchers and the technical review panel (listed in the Acknowledgments) for the project collaborate to craft a plan to implement the study recommendations and to determine the benefits of doing so. This process is to ensure that the implementation plan is developed and approved with the participation and support of those involved with VDOT operations. The implementation plan and the accompanying benefits are provided here.

Implementation

Regarding Recommendation 1, VTRC, with support from VDOT's Materials Division, will develop a Research Needs Statement by December 2026 to collect additional response data from Segments II and III.

Regarding Recommendation 2, VTRC, with support from VDOT's Materials Division, will develop a Research Needs Statement by December 2026 to investigate if the design of similar pavement structures can be further optimized. In addition, VTRC recently initiated a research project to investigate the in-place properties of FDR, the results of which can be used to support implementing this recommendation.

Regarding Recommendation 3, VTRC will provide District Materials and Maintenance staff with supporting information on the benefits of using pavement recycling techniques in deep repair and reconstruction projects and will help identify candidate projects by May 2027. Implementation funds may be considered to offset delta costs for potential future projects.

Benefits

The work conducted through this research project was an extension of full-scale accelerated pavement testing conducted at NCAT at Auburn University. VDOT sponsored three test sections that included CCPR (one of which also included FDR), which were trafficked between 20 and 40 million ESALs for 6 to 12 years. Several publications derived from this study documented the performance of these sections and showed the potential for long-life pavement performance in a research setting (Bowers et al., 2024; Diefenderfer et al., 2019; Timm et al., 2015; Timm et al., 2018). Segments II and III on I-64 showed that these ideas could be extended and applied in a real-world application.

By using the pavement recycling techniques on Segments II and III, VDOT derived more than $15 million in cost savings. This figure was calculated by comparing the contractor's bid for the pavement recycling design with VDOT's estimates for conventional pavement materials. When considering the costs of the research work at NCAT from 2012 to 2021, the benefit-to-cost ratio was approximately 3.7:1. In addition to cost savings, an FHWA published report documented environmental savings from the recycling processes used on the I-64 projects. The FHWA report stated that the recycling techniques reduced the initial construction energy demand by up to 45% and reduced the greenhouse gas emissions by up to 40% (FHWA, 2020).

The benefit of implementing Recommendation 1 is that VDOT and other departments of transportation can better predict the longer term performance of recycled pavement sections and make better design decisions on future projects. In addition, collecting additional data will confirm if these pavement sections are long-life pavement sections, and if so, the design concepts can be used on future projects in which further cost savings can be realized. Long-life pavements are characterized by lower life-cycle costs.

The benefit of implementing Recommendation 2 is that VDOT may realize further cost benefits from using recycled pavement sections by optimizing the design. The results of this study showed very low strain levels, below commonly reported threshold values for indefinite fatigue life. A preliminary layered elastic analysis revealed that the cross section could be further optimized with minimal increase in strain at the bottom of the asphalt layers and stress at the bottom of the FDR layer, achieving a materials cost savings of up to 12%. Some of this work is part of a recently initiated research project to investigate the in-place properties of FDR.

The benefit of implementing Recommendation 3 is the potential for VDOT to experience increased pavement service lives. The performance for a similar pavement design used on the I-81 project completed in 2011 shows good service with condition index values ranging from 100 to 80 and low and steady international roughness index values (less than 50 inches per mile) after nearly 14 years of service. Figure 22 shows the load-related distress rating, nonload-related distress rating (NDR), and international roughness index from 2012 (the year after construction)

to 2025. The maximum values for load-related distress rating and NDR are 100. Figure 22 shows that the load-related distress rating ranges from the mid-90s to 100. NDR ranges from the low 80s to 100. The increases in NDR in 2024 and 2025 reflect sealing the longitudinal joint between the two travel lanes.

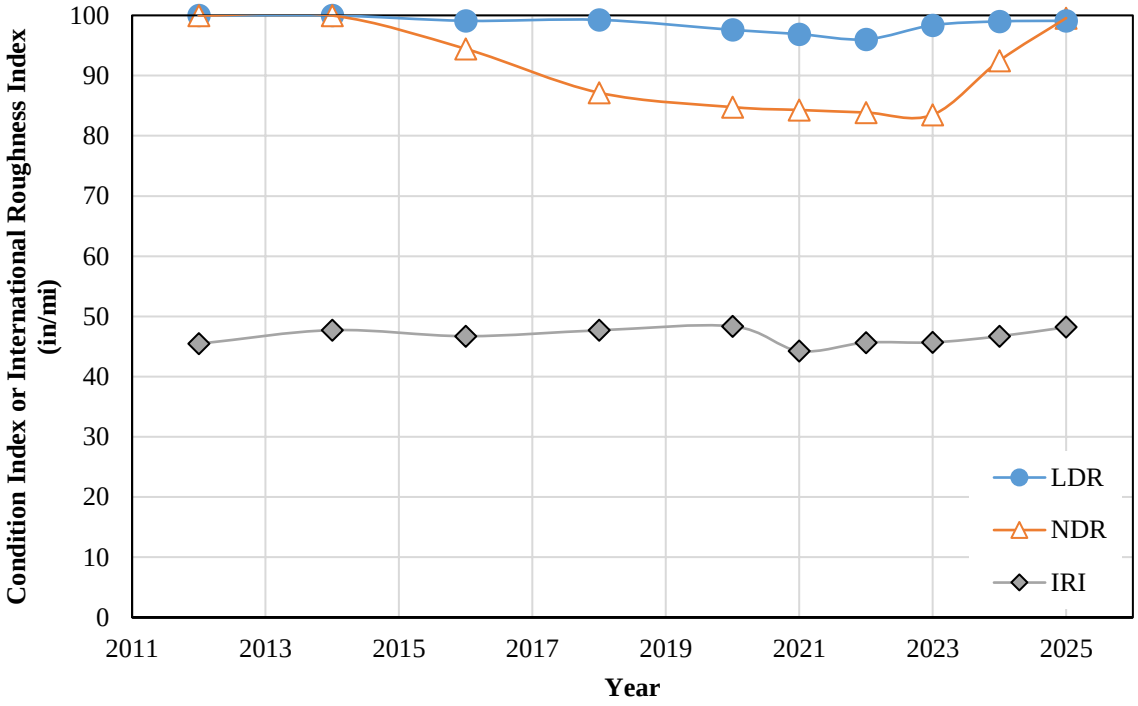

Figure 222. LDR Rating, NDR Rating, and IRI for Interstate 81 Recycling Project from 2012 to 2025. IRI = international roughness index; LDR = load-related distress; NDR = nonload-related distress.

The right lane of the I-81 recycling project has carried nearly 35 million ESALs as of the writing of this report. Current traffic data for Segments II and III on I-64 show that these sections accumulate ESALs at approximately 0.6 to 1.1 million ESALs per year, depending on location. Section S12, constructed on the NCAT Test Track in 2012 and tested until 2021, carried approximately 30 million ESALs on a thinner pavement section with similar good performance, and no signs of distress were evident on the pavement surface when trafficking was discontinued. Current VDOT pavement management system data show that Segments II and III are initially performing, as well as the initial performance periods of the I-81 project.

ACKNOWLEDGMENTS

The authors are grateful to the following individuals who served on the technical review panel for this study: Miranda Kidd (champion) and James Peavy, VDOT Hampton Roads District; Kwame Adu-Gyamfi and Thomas Schinkel, VDOT Richmond District; and Girum Merine and Bipad Saha, VDOT Materials Division. The authors also thank Tom Tate, formerly of VDOT; Billy Hobbs, Richard Mejia, and David Songer of Virginia Tech Transportation Institute; and Fabrizio Meroni, Kenny Smith, Max Ratcliffe, and Wenjing Xue, formerly of Virginia Tech Transportation Institute, for their assistance with this study.

REFERENCES

Amarh, E.A. *Evaluating the Mechanical Properties and Long-Term Performance of Stabilized Full-Depth Reclamation Base Materials.* Master's thesis. Virginia Tech, Blacksburg, VA, 2017.

Benavides-Ruiz, C. *Instrumented Response and Multilayer Modeling of Cold Central Plant Recycled Pavement Section.* Master's thesis. Virginia Tech, Blacksburg, VA, 2021.

Bowers, B.F., Diefenderfer, B.K., Cross, S.A., Nordcbeck, A.V., and Gu, F. *Construction of Cold Central Plant Recycling and Cold In-Place Recycling of Asphalt Pavements Best Practices Guide.* Project No. 14-43. National Center for Asphalt Technology, Auburn, AL, 2022.

Bowers, B.F., Diefenderfer, B.K., and Kazmi, S. *Stockpiling Cold Central Plant Recycling Mixtures*. Report No. FHWA/VTRC 19-R32. Virginia Transportation Research Council, Charlottesville, VA, 2019.

Bowers, B.F., Lynn, T., Timm, D.H., Diefenderfer, B.K., and Gatiganti, S.C. Long-Term Performance and Forensic Evaluation of an Asphalt Pavement with Cold Central Plant Recycled Asphalt. *Transportation Research Record*, Vol. 2678, No. 4, April 2024, pp. 917–931.

Bressi, S., Fiorentini, N., Huang, J., and Losa, M. Crumb Rubber Modifier in Road Asphalt Pavements: State of the Art and Statistics. *Coatings,* Vol. 9, No. 6, June 2019, p. 384.

Bruns, T. Widening Project in Coastal Virginia Uses Innovative Recycling Materials. *Roads & Bridges,* February 2021. https://www.roadsbridges.com/widening-project-coastal-virginia-uses-innovative-recycling-materials.

Chavez, F., Marcobal, J., and Gallego, J. Laboratory Evaluation of the Mechanical Properties of Asphalt Mixtures with Rubber Incorporated by the Wet, Dry, and Semi-Wet Process. *Construction and Building Materials,* Vol. 205, April 2019, pp. 164–174.

Decagon Devices, Inc. *GS1 Soil Moisture Sensor: Operator's Manual.* Pullman, WA, 2015.

Diefenderfer, B.K., Apeagyei, A., Gallo, A.A., Dougald, L.E., and Weaver, C.B. In-Place Pavement Recycling on I-81 in Virginia. *Transportation Research Record,* Vol. 2306, December 2012, pp. 21–27.

Diefenderfer, B.K, Bowers, B.F., Schwartz, C.W., Farzaneh, A., Zhang, Z. Dynamic Modulus of Recycled-Pavement Mixtures. *Transportation Research Record*, Vol. 2575, No. 1, 2016a, pp. 19–26.

Diefenderfer, B.K., Flintsch, G., Xue, W., Meroni, F., Boz, I., and Timm, D. Structural Performance of an Asphalt Pavement Containing Cold Central Plant Recycling and Full-

Depth Reclamation. *Transportation Research Record,* Vol. 2677, No. 1, January 2023, pp. 409–419.

Diefenderfer, B.K., Díaz Sánchez, M., Timm, D.H., and Bowers, B.F. *Structural Study of Cold Central Plant Recycling Sections at the National Center for Asphalt Technology (NCAT) Test Track.* VTRC-17-R9. Virginia Transportation Research Council, Charlottesville, VA, 2016b.

Diefenderfer, B.K., Timm, D.H., and Bowers, B.F. *Structural Study of Cold Central Plant Recycling Sections at the National Center for Asphalt Technology (NCAT) Test Track: Phase II*. VTRC-19-R25. Virginia Transportation Research Council, Charlottesville, VA, 2019.

Federal Highway Administration. *In-Place and Central Plant Recycling of Asphalt Pavements in Virginia*. FHWA-HIF-19-078. Federal Highway Administration, Washington, DC, 2020.

Federal Highway Administration. Asphalt Pavement Recycling with Reclaimed Asphalt Pavement (RAP), 2022. https://www.fhwa.dot.gov/pavement/recycling/rap/#:~:text=Asphalt%20Pavement%20Recycling%20Technologies%20A,(ARRA)%2C%20and%20the%20National.

Flintsch, G., Xue, W., Diefenderfer, B.K., and Meroni, F. Evaluation of Cold Central Plant Recycling Technique Using Full-Scale Accelerated Pavement Testing. In *Accelerated Pavement Testing to Transport Infrastructure Innovation,* 6th International Conference on Accelerated Pavement Testing. Springer, Singapore, 2020, pp. 270–279.

Hajek, J.J., Kazmierowski, T.J., Sturm, H., Bathurst, R.J., and Raymond, G.P. Field Performance of Open-Graded Drainage Layers. *Transportation Research Record,* Vol. 1354, No. 1, January 1992, pp. 55–64.

Hossain, M.S. *Characterization of Unbound Pavement Materials From Virginia Sources for Use in the New Mechanistic-Empirical Pavement Design Procedure.* FHWA/VTRC 11-R6. Virginia Transportation Research Council, Charlottesville, VA, 2010.

Jain, S., and Singh, B. Cold-Mix Asphalt: An Overview. *Journal of Cleaner Production,* Vol. 280, No. 2, 2021.

Liu, X., Cui, Q., and Schwartz, C. Performance Benchmark of Greenhouse Gas Emissions from Asphalt Pavement in the United States. In *International Conference on Sustainable Infrastructure 2014: Creating Infrastructure for a Sustainable World.* American Society of Civil Engineers, Reston, VA, 2014. pp. 678–689.

Moreno-Navarro, F., Rubio Gámez, M.C., and Jiménez del Barco Carrión, A. Tire Crumb Rubber Effect on Hot Bituminous Mixtures Fatigue-Cracking Behavior. *Journal of Civil Engineering and Management,* Vol. 22, No. 1, October 2015, pp. 65–72.

National Centers for Environmental Information. *National Monthly Climate Report for November 2021*, Washington, DC, 2021. https://www.ncei.noaa.gov/access/monitoring/monthly-report/national/202111.

OpenPave. Open source pavement engineering software, 2025. https://openpave.org. Accessed May 7, 2025.

Reeder, G.D., Harrington, D.S., Ayers, M.E., and Adaska, W. *Guide to Full-Depth Reclamation (FDR) with Cement.* SR1006P. National Concrete Pavement Technology Center, Ames, IA, 2019.

Díaz Sánchez, M.A. *Structural Characterization of Recycled Materials at the NCAT Test Track*. Ph.D. dissertation. Auburn University, Auburn, AL, 2019.

Smith, B.C., and Diefenderfer, B.K. *Development of Truck Equivalent Single-Axle Load (ESAL) Factors Based on Weigh-in-Motion Data for Pavement Design in Virginia.* VTRC 09-R18. Virginia Transportation Research Council, Charlottesville, VA, 2009.

Timm, D.H. Temperature Normalization of Flexible Pavement Response Measurements. In *Accelerated Pavement Testing to Transport Infrastructure Innovation*. Springer, Cham, Switzerland, 2020, pp. 574–582.

Timm, D.H., Diefenderfer, B.K., and Bowers, B.F. Cold Central Plant Recycled Asphalt Pavements in High-Traffic Applications. *Transportation Research Record*, Vol., 2672, No. 40, October 2018, pp. 291–303.

Timm, D.H., Sánchez, M.D., and Diefenderfer, B.K. *Field Performance and Structural Characterization of Full-Scale Cold Central Plant Recycled Pavements.* No. 15-0781. Transportation Research Board, Washington, DC, 2015.

Tran, N., Robbins, M.R., Timm, D.H., Willis, J.R., and Rodezno, C. *Refined Limiting Strain Criteria and Approximate Ranges of Maximum Thicknesses for Designing Long-Life Asphalt Pavements.* NCAT Report 15-05R. National Center for Asphalt Technology, Auburn, AL, 2016.

Virginia Department of Transportation. *AASHTOWare Pavement ME User Manual*. Materials Division, Pavement Design and Evaluation, Sandston, VA, 2017.

Virginia Department of Transportation. Pavement Recycling: Segments II and III, 2019. https://i64widening.org/learn_more/pavement_recycling_methods.asp#:~:text=VDOT%20is%20utilizing%20environmentally%2Dfriendly,Recycling%20and%20Full%20Depth%20Reclamation. Accessed June 20, 2022.

West, R., Powell, R., Timm, D.H., Tran, N., Yin, F., Moore, N., Harman, T., Bowers, B.F., Vargas, A., Rodezno, C., Puchalski, R.M., Chen, C., Gatiganti, S.C., Nelson, J., Julian, G., Moore, J., Taylor, A., Turner, P., Kmetz, M., and Turochy, E. *Phase VIII (2021–*

2024) NCAT Test Track Findings. NCAT Report 24-01. National Center for Asphalt Technology, Auburn, AL, 2024.

Williams, B., Willis, J., and Ross, T. *Asphalt Pavement Industry Survey on Recycled Materials and Warm-Mix Asphalt Usage 2018.* Information Series 138. National Asphalt Pavement Association, Greenbelt, MD, 2019.

Zimmerman, C. *Performance Analysis and Modeling of Pavements with a Cold Central Plant Recycled Base Under Accelerated Loading Testing*. Master's thesis. VirginiaTech, Blacksburg, VA, 2017.

APPENDIX A: CONSTRUCTION AND INSTALLATION

Figure A1. Pavement Section before Construction (September 27, 2018)

Figure A2. Excavation

Figure A3. Instrumentation—Pressure Cell

Figure A4. Backfilling

Figure A5. Subgrade Layer Placed after Excavation (October 16, 2018)

APPENDIX B: INSTRUMENTATION DEVICES

The pavement section was instrumented with asphalt strain gauges, earth pressure cells, and thermocouples to quantify pavement responses.

Table B1 summarizes the instruments and data acquisition modules used in this experiment. All sensors were checked before installation to ensure that they corresponded to external stimulations as expected.

Table B1. Equipment Used

		Functionality	Manufacturer	Model	Capacity
DAS	Chassis	Accommodate modules	National Instruments Corporation	PXle-1082	8 slots
	Controller	Control DAS		PXle-8840	2.6 GHz
	Module	Collect signals from pressure cells		PXle-6361	16 channels
	Module	Collect signals from thermocouples		PXle-4353	32 channels
	Module	Collect signals from strain gauges		PXle-4330	8 channels
	Module	Collect signals from strain gauges		PXle-4339	8 channels
Strain Gage		Measure dynamic deformation in pavement	Tokyo Sokki Kenkyujo Co., Ltd.	KM-100HAS	$\pm 5000 \times 10^{-6}$
Pressure Cell		Measure dynamic pressure in pavement	Geokon, Inc.	3500	0~250 kPa
Thermocouple		Measure temperature in pavement	Pyromation, Inc.	T	–200~370°C

DAS = data acquisition system.

Data Acquisition System

A data acquisition system from National Instruments Corporation was acquired to collect signals from the pavement instrumentation (Figure B1). The system is housed in an 8-slot chassis (model NI PXle-1082), which features a high-bandwidth backplane to meet a wide range of high-performance test and measurement application needs. Slots were filled with modules and storage cards based on the type of sensors embedded in the pavement. A program was developed in LabVIEW to acquire, analyze, present, and manage the measured data.

Figure B1. Data Acquisition System

Strain Gauges

Strain transducers (model KM-100HAS, produced by Tokyo Sokki Kenkyujo Co., Ltd.), shown in Figure B2, and a Tokyo Sokki strain gauge were used to measure the dynamic deformation of the pavement structures. This strain gauge model is both heat resistant and waterproof, and its reinforcing bars ensure a strong fixation in the asphalt concrete layer. Pavement strain is measured through a spring element protected by a metallic pipe and fluoroplastic tape, converted into electrical signals and then sent to the data acquisition system.

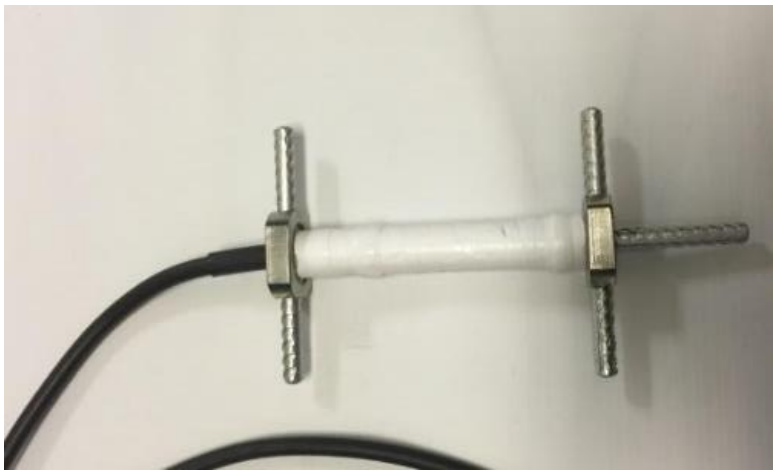

Figure B2. Tokyo Sokki Strain Gauge

Pressure Cells

GeoKon 3500 series Earth pressure cells, shown in Figure B3, were used to measure the pressure distribution in the subgrade layer. These pressure cells use a semiconductor-type

pressure transducer to measure dynamic stress changes and thus have the advantages of long-term stability, reliable performance with long cables, and insensitivity to moisture intrusion.

Figure B3. Geokon 3500 Pressure Cell

The pressure cells include a thermistor for temperature measurement and a gas discharge tube for lightning protection. They have a high accuracy (5%) because of their large diameter-to-thickness ratio (greater than 10). These cells feature an output of 2 mV/V, 0–5 VDC, or 4–20 mA and have been widely applied to measure traffic-induced stresses on roadway subgrades, airport runways, and under railroad tracks.

Thermocouples

Thermocouples produced by Pyromation, Inc. (model TP33U-04-00-T3A300-012-3), shown in Figure B4, were installed to measure the temperature within and outside the pavement sections. The thermocouples obtained the temperature value using the voltage created (electro-motive force) by using the presence of two dissimilar metals.

Figure B4. Pyromation T-Type Thermocouple

Moisture Sensor

The moisture sensor (Figure B5), the Model GS1 developed by Decagon Devices, Inc., was used in this experiment to measure the moisture content in pavement. This sensor determines volumetric water content by measuring the dielectric constant of the medium using capacitance and frequency domain technology. The two-prong design allows the sensor to measure volumetric water content from 0 to 57%. The volumetric water content of saturated soils is generally 40 to 50% depending on the soil type. The measurement frequency can be 70 MHz at most.

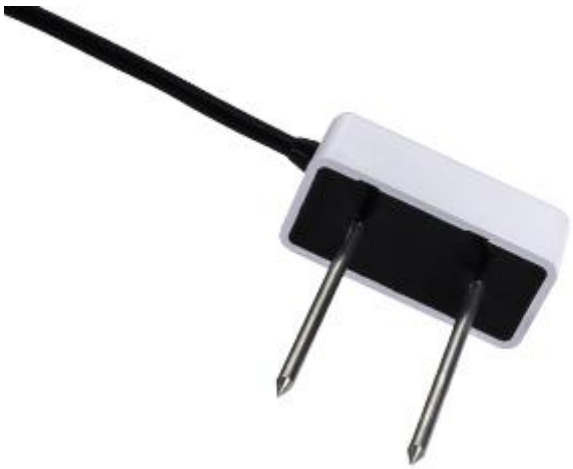

Figure B5. Soil Moisture Sensor Decagon Devices GS1. Image retrieved from Decagon Devices, Inc. (2015)

APPENDIX C: TRUCK WEIGHT RECORDS

Table C1. Truck Weight Records

Test	Date	Ref.	Axle	Left (lbs.)	Right (lbs.)	Total Axle (lbs.)	Total Truck (lbs.)
1	Jun 2019	R16025	1	5,600	5,500	11,100	31,100
			2	10,000	10,000	20,000	
		R14058	1	6,500	6,000	12,500	44,700
			2	8,000	8,000	16,000	
			3	8,200	8,000	16,200	
		R16213	1	6,800	6,600	13,400	45,600
			2	8,000	8,000	16,000	
			3	8,200	8,000	16,200	
2	Aug 2019	**R15178**	1	5,850	5,900	11,750	34,000
			2	11,500	10,750	22,250	
		R16046	1	5,450	5,100	10,550	29,850
			2	9,650	9,650	19,300	
		R16213	1	6,550	6,500	13,050	44,750
			2	8,000	7,600	15,600	
			3	8,300	7,800	16,100	
3	Sep 2019	**R6306**	1	4,900	4,600	9,500	29,800
			2	10,000	10,300	20,300	
		R16075	1	5,800	5,400	11,200	30,900
			2	10,300	9,400	19,700	
		R16046	1	5,400	5,000	10,400	30,300
			2	9,900	10,000	19,900	
4	Nov 2019	R16046	1	6,100	5,200	11,300	30,100
			2	9,000	9,800	18,800	
		R15178	1	5,700	5,400	11,100	30,900
			2	10,000	9,800	19,800	
		R14155	1	7,600	7,200	14,800	44,600
			2	7,500	7,300	14,800	
			3	7,800	7,200	15,000	
5	Dec 2019	**R16046**	1	6,000	5,300	11,300	33,700
			2	12,000	10,400	22,400	
		R15178	1	5,800	5,500	11,300	29,500
			2	9,400	8,800	18,200	
		R16075	1	5,800	5,400	11,200	30,500
			2	10,200	9,100	19,300	
6	Apr 2021	R16075	1	5,800	5,600	11,400	31,500
			2	9,900	10,200	20,100	
		R16046	1	5,800	5,800	11,600	32,500
			2	10,500	10,400	20,900	
		R21085	1	5,900	5,300	11,200	31,900
			2	11,000	9,700	20,700	
		R15178	1	6,200	5,400	11,600	32,500
			2	11,500	9,400	20,900	
7	Nov 2021	**R16214**	1	6,600	6,300	12,900	41,800
			2	7,800	7,100	14,900	
			3	7,400	6,600	14,000	
		R2222	1	7,500	6,900	14,400	43,300
			2	7,500	7,100	14,600	

Test	Date	Ref.	Axle	Left (lbs.)	Right (lbs.)	Total Axle (lbs.)	Total Truck (lbs.)
			3	7,400	6,900	14,300	
		R14155	1	7,300	7,000	14,300	42,000
			2	6,800	7,200	14,000	
			3	6,900	6,800	13,700	
8	Apr 2022	R21085	1	5,700	5,300	11,000	28,900
			2	9,400	8,500	17,900	
		R14056	1	5,800	5,300	11,100	29,700
			2	9,300	9,300	18,600	
		R19065	1	7,200	6,800	14,000	42,200
			2	7,600	6,600	14,200	
			3	7,400	6,600	14,000	
9	Aug 2022	R16213	1	7,100	7,100	14,200	44,200
			2	7,100	7,700	14,800	
			3	8,100	7,100	15,200	
		R14155	1	7,100	6,300	13,400	44,000
			2	7,200	8,000	15,200	
			3	7,500	7,900	15,400	
		R16046	1	5,800	5,200	11,000	31,100
			2	10,600	9,500	20,100	
10	Nov 2022	R15178	1	5,800	5,500	11,300	36,300
			2	10,000	15,000	25,000	
		R21085	1	5,800	5,400	11,200	30,900
			2	10,000	9,700	19,700	
		R14155	1	7,000	7,400	14,400	41,600
			2	6,500	7,500	14,000	
			3	6,500	6,700	13,200	
11	Mar 2023	R14155	1	7,900	7,100	15,000	43,900
			2	7,700	6,700	14,400	
			3	7,900	6,600	14,500	
		R18099	1	5,800	5,500	11,300	31,900
			2	10,800	9,800	20,600	
		R16045	1	6,100	5,600	11,700	31,300
			2	10,200	9,400	19,600	
12	Aug 2023	R23112	1	7,300	7,600	14,900	44,200
			2	7,300	7,400	14,700	
			3	7,700	6,900	14,600	
		R16075	1	5,800	5,600	11,400	30,700
			2	10,300	9,000	19,300	
		R14152	1	6,900	7,000	13,900	43,500
			2	8,000	7,000	15,000	
			3	8,100	6,500	14,600	
13	Nov 2023	R14155	1	5,300	5,500	10,800	30,500
			2	9,400	10,300	19,700	
		R15178	1	5,900	5,500	11,400	31,100
			2	10,000	9,700	19,700	
		R14155	1	7,200	7,400	14,600	43,400
			2	7,300	7,100	14,400	
			3	8,000	6,400	14,400	

APPENDIX D: AIR AND PAVEMENT TEMPERATURE RELATIONSHIP

Because temperature data from the embedded sensors were not recorded during one of the field experiments, a linear regression analysis was conducted using the average air temperature on the experiment date, the average air temperature from the previous day, and the sensor depth for both segments. Equation D1 and Figure D1 illustrate the relationship between air temperature and pavement temperature, with the regression exhibiting a strong correlation (R2 = 0.94).

$$Pavement\ Temp = 0.5349 Air\ Temp_{day} + 0.6080 Air\ Temp_{day-1} - 0.6704 Depth + 5.6271 \quad \text{Equation D1}$$

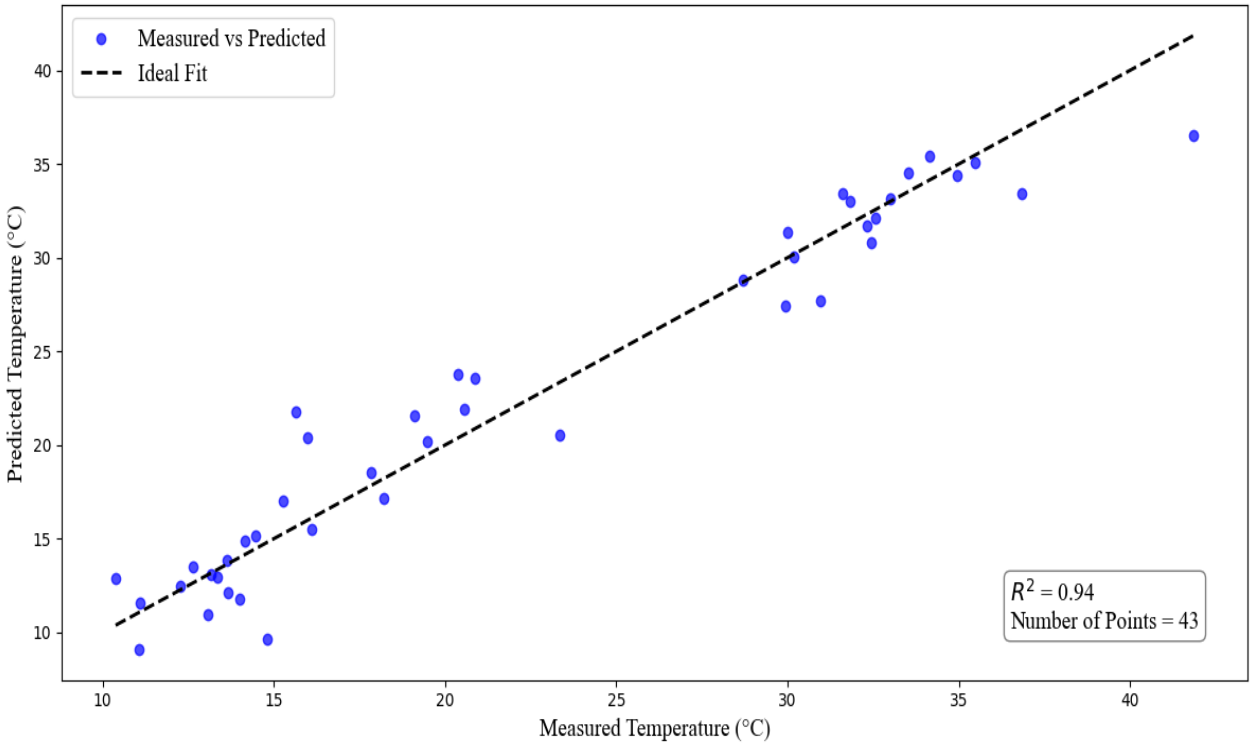

Figure D1. Linear Relationship between Air and Pavement Temperature

APPENDIX E: STRAIN—TEMPERATURE NORMALIZING

Exponential trend lines were developed for the data collected by each axle type, and the tensile microstrain at 20°C (68°F) was obtained following Equation E1.

$$\varepsilon_{TR} = \varepsilon_T \times e^{k_2 \times (T_R - T)} \qquad \text{Equation E1}$$

Where:

ε_{TR} = tensile microstrain measured at reference temperature TR.
ε_T = tensile microstrain measured at temperature T.
e = exponential constant.
k_1, k_2 = regression coefficients.
T_R = reference mid-depth pavement temperature (°C).
T = mid-depth pavement temperature (°C).

Segment II

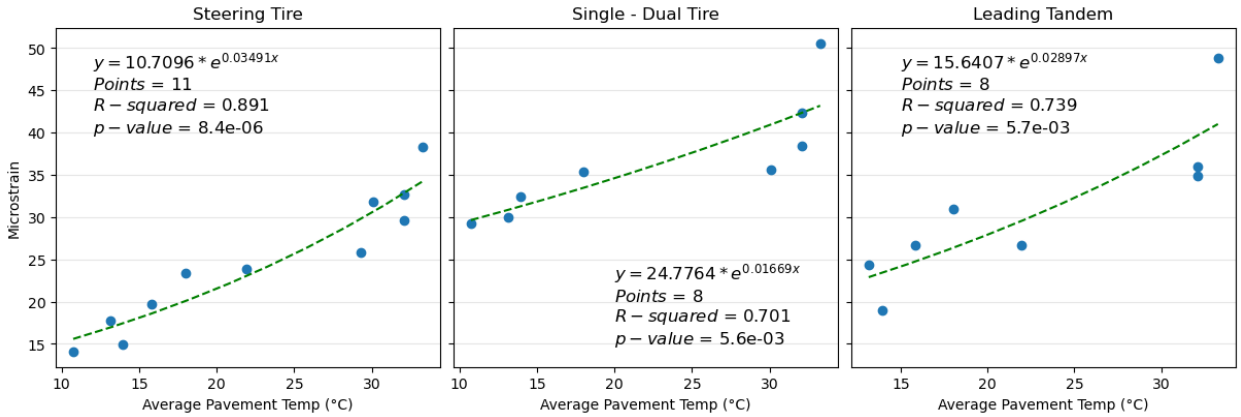

Figure E1. Total Strain Responses and Average Pavement Temperature Relationship–Segment II

Segment III

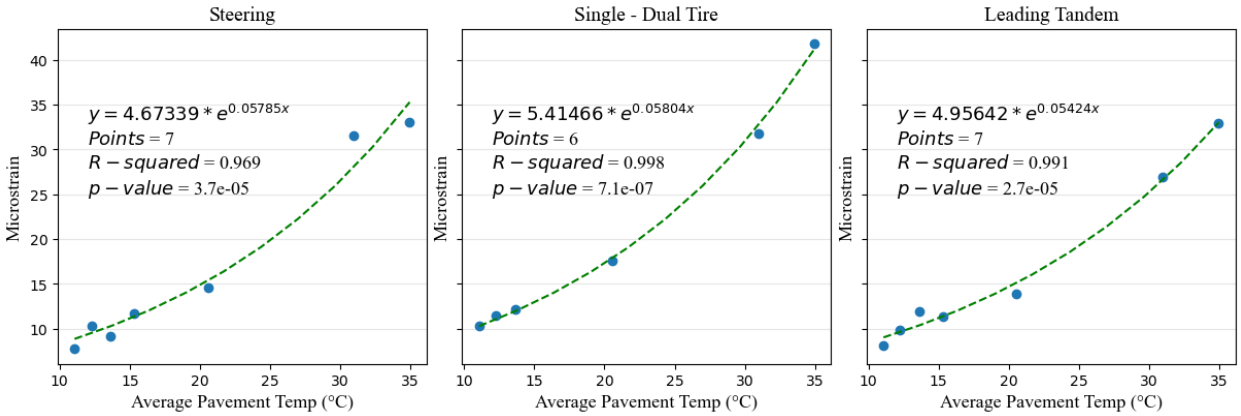

Figure E2. Total Strain Responses and Average Pavement Temperature Relationship–Segment III

Segment II

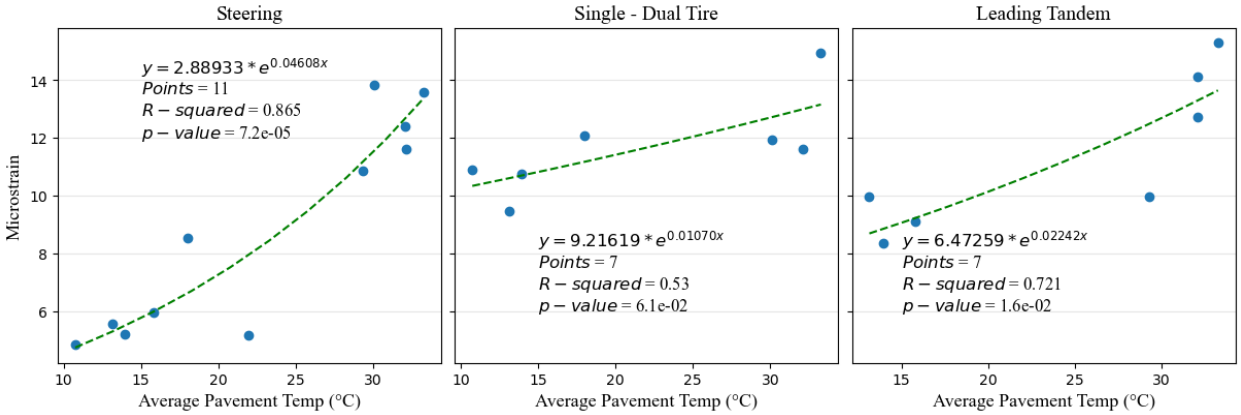

Figure E3. Tensile Strain Responses and Average Pavement Temperature Relationship–Segment II

Segment III

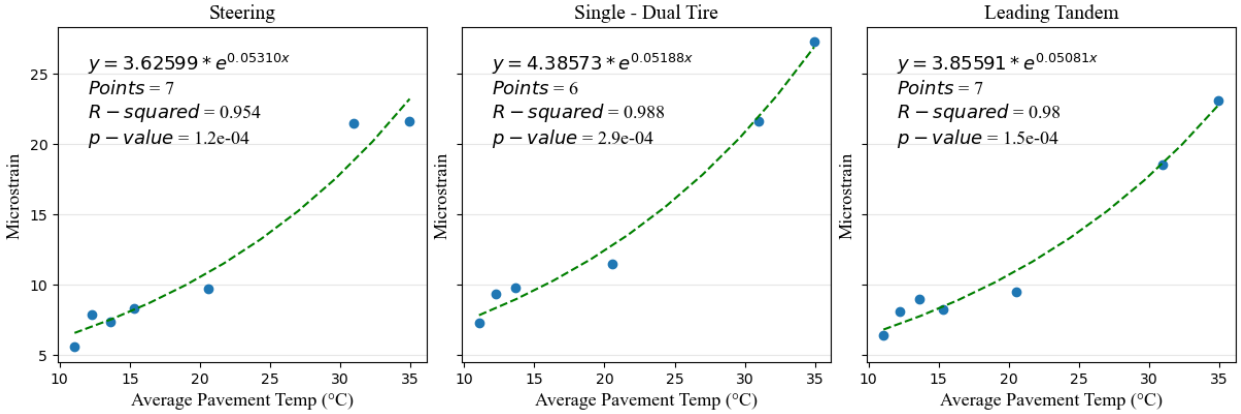

Figure E4. Tensile Strain Responses and Average Pavement Temperature Relationship–Segment III

APPENDIX F: TRAFFIC ESTIMATION

Segment II of the Interstate 64 project begins west of Route 199 (Humelsine Parkway and Marquis Center Parkway) near Exit 242 and concludes east of Route 238 near Exit 247. (VDOT, 2019). Historical data on the average number and types of vehicles were extracted by utilizing two primary sources:

- The Virginia Traffic Volume Map available at https://www.arcgis.com/apps/webappviewer/index.html?id=35e4c06de0f84a9c9f3fe18e67cd2c92.
- The online traffic data publications provided by VDOT accessible at https://www.vdot.virginia.gov/doing-business/technical-guidance-and-support/traffic-operations/traffic-counts/.

The Virginia Traffic Volume Map was used to identify the specific route name, and VDOT publications were used to obtain the annual average daily traffic from 2017 to 2021 (Table F1).

Table F1. Interstate 64 Traffic

	Historic Volume							
Year	**AADT**	**Vehicles**	**Buses**	**SUT2**	**SUT3**	**CT1T**	**CT2T**	**ESALs**
2017	41,000	95.5%	0.6%	0.6%	0.5%	2.7%	0.1%	1,533
2018	42,000	95.5%	0.6%	0.6%	0.5%	2.7%	0.1%	1,546
2019	43,000	95.6%	0.6%	0.6%	0.5%	2.6%	0.1%	1,566
2020	36,000	95.0%	0.5%	0.7%	0.6%	3.1%	0.1%	1,497
2021	44,000	95.1%	0.4%	0.8%	0.6%	3.0%	0.1%	1,811

AADT = annual average daily traffic; CT1T = combination trucks 1 trailer year; CT2T = combination trucks 2+ trailer year; ESALs = equivalent single-axle loads; SUT2 = single-unit trucks two-axle; SUT3 = single-unit trucks three-axle.

The route identified to analyze the traffic is Route R-VA IS00064WB (Link ID 150045), spanning from State Route 199 East, Humelsine Parkway, to U.S. Route 60 Pocahontas Trail: State Route 143 Merrimac Trail.

Given the significance of estimating the number of equivalent single-axle loads (ESALs) the pavement structure will be subjected to during its design life, the Virginia Vehicle ESAL Factor for Flexible Pavement was consulted (Smith and Diefenderfer, 2009). For passenger vehicles, single-unit trucks (FHWA Classes 4–7), and combination trucks (FHWA Classes 8–13), the respective values of 0.0002, 0.46, and 1.05 were applied. Researchers used Equation F1 to calculate ESALs per year:

$$ESAL_i = AADT_i \times \left[(\%Vehicles_i \times 0.0002) + \left((\%Buses_i + \%SUT2_i + \%SUT3_i) \times 0.46\right) + \left((\%CT1T_i + \%CT2T_i) \times 1.05\right)\right] \quad \text{Equation F1}$$

Where:
$ESAL_i$ = ESALs year i.
$AADT_i$ = Annual average daily traffic year i.
$\%Vehicles_i$ = Percent of passenger cars year i.

$\%Buses$ = Percent of buses year i.
$\%SUT2_i$ = Percent of single-unit trucks 2-axle year i.
$\%SUT3_i$ = Percent of single-unit trucks +3-axle year i.
$\%CT1T_i$ = Percent of combination trucks 1 trailer year i.
$\%CT2T_i$ = Percent of combination trucks 2+ trailer year i.

Considering that the annual average daily traffic used in the model corresponds to traffic in one direction, the directional distribution factor (D) remains at 1.0. In addition, this part of Interstate 64 has a three-lane configuration. Therefore, D is assumed to be 0.8. A growth rate of 2.5% was adopted, reflecting the observed pattern from 2017 to 2019.

Then, the design ESALs are calculated using Equation F2:

$$ESALs = ESALs_{2019} \times \frac{(1+r)^Y - 1}{r} \times D \times L \times 365 \qquad \text{Equation F2}$$

Table F2 presents the ESALs estimations from 2019 to 2023 for Segments II and III.

Table F2. Equivalent Single-Axle Load Estimation

	Date	Days	Years	ESALs
SEGMENT II	**26 June 2019**	76	0.208	94,264
	15 August 2019	126	0.345	156,544
	11 September 2019	153	0.419	190,263
	06 November 2019	209	0.573	260,396
	18 December 2019	251	0.688	313,170
	27 April 2021	747	2.047	947,883
	18 November 2021	952	2.608	1,216,498
	07 April 2022	1,092	2.992	1,402,095
	18 August 2022	1,225	3.356	1,580,047
	15 November 2022	1,314	3.600	1,700,026
	22 March 2023	1,441	3.948	1,872,487
	16 August 2023	1,588	4.351	2,073,966
	15 November 2023	1,679	4.600	2,199,699
SEGMENT III	**17 November 2021**	12	0.033	14,852
	06 April 2022	152	0.416	189,013
	17 August 2022	285	0.781	356,002
	16 November 2022	376	1.030	471,126
	21 March 2023	501	1.373	630,424
	15 August 2023	648	1.775	819,489
	14 November 2023	739	2.025	937,476

APPENDIX G: STRESS—TEMPERATURE ADJUSTMENT

Segment II—Cold Central Plant Recycling

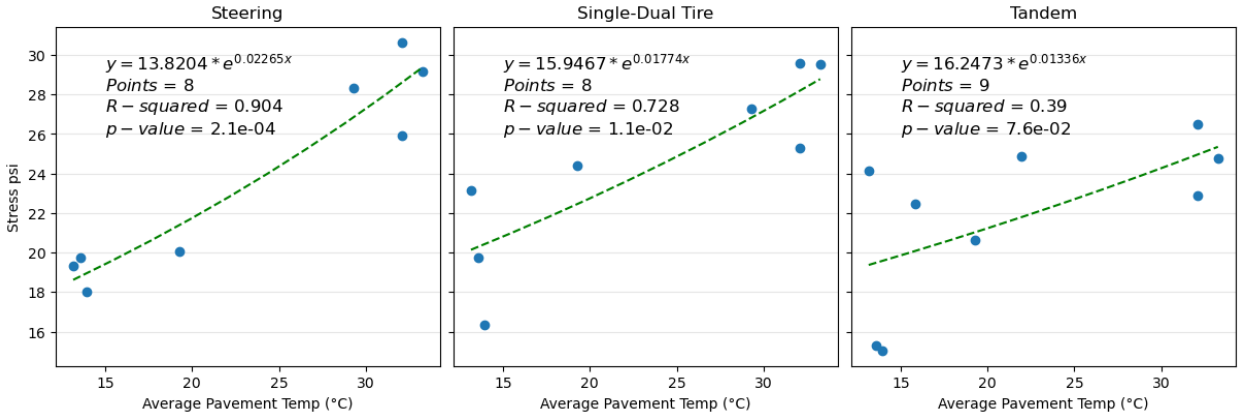

Figure G1. Bottom Cold Central Plant Recycling Stress Responses and Average Pavement Temperature Relationship–Segment II

Segment II—Subgrade

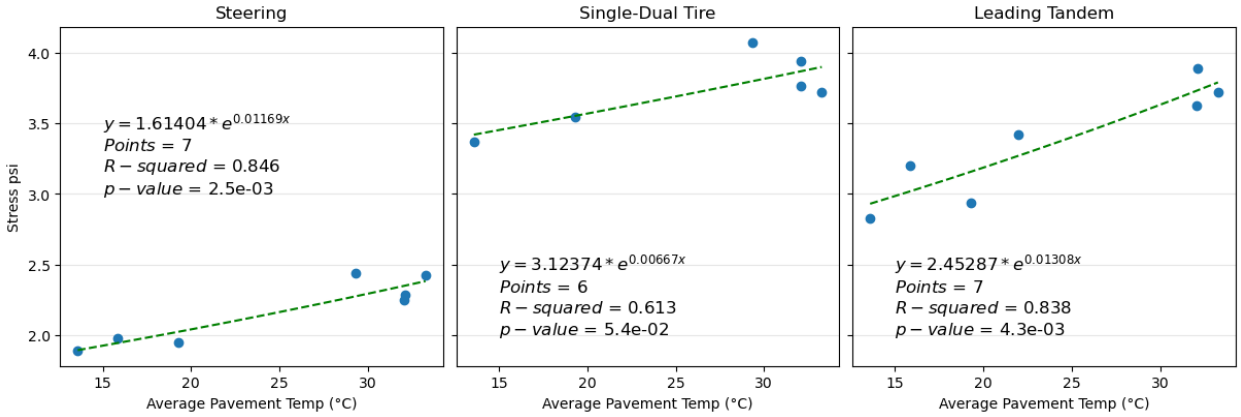

Figure G2. Top Subgrade Stress Responses and Average Pavement Temperature Relationship–Segment II

Segment III—Subgrade

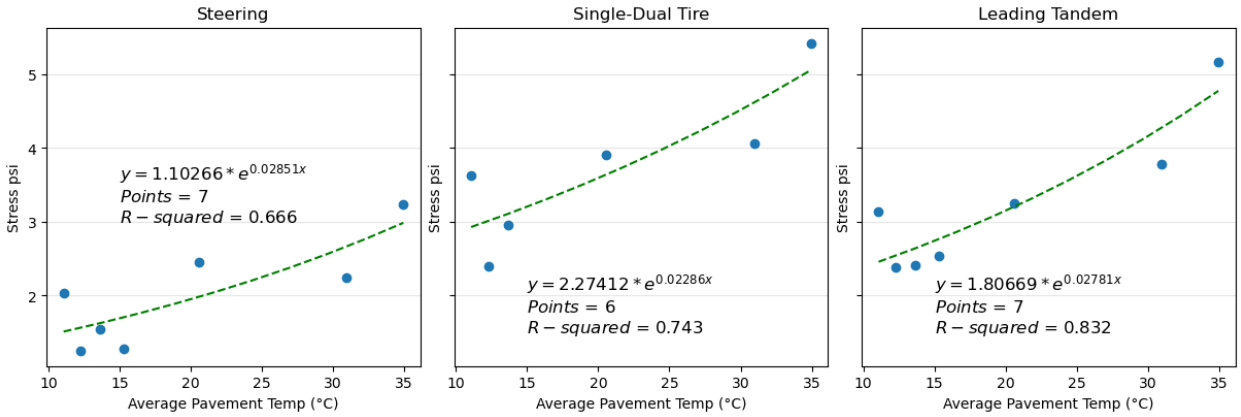

Figure G3. Top Subgrade Stress Responses and Average Pavement Temperature Relationship–Segment III